

NASA MEMO 5-5-59W

JN-3-1
374410

NASA

MEMORANDUM

EFFECT OF CONTRACTION ON TURBULENCE AND TEMPERATURE
FLUCTUATIONS GENERATED BY A WARM GRID

By Robert R. Mills, Jr., and Stanley Corrsin

The Johns Hopkins University

**NATIONAL AERONAUTICS AND
SPACE ADMINISTRATION**

WASHINGTON

May 1959

NATIONAL AERONAUTICS AND SPACE ADMINISTRATION

MEMORANDUM 5-5-59W

EFFECT OF CONTRACTION ON TURBULENCE AND TEMPERATURE

FLUCTUATIONS GENERATED BY A WARM GRID

By Robert R. Mills, Jr., and Stanley Corrsin

SUMMARY

Hot-wire anemometer measurements were made of several statistical properties of approximately homogeneous and isotropic fields of turbulence and temperature fluctuations generated by a warm grid in a uniform airstream sent through a 4-to-1 contraction. These measurements were made both in the contraction and in the axisymmetric domain farther downstream.

In addition to confirming the well-known turbulence anisotropy induced by strain, the data show effects on the skewnesses of both longitudinal velocity fluctuation (which has zero skewness in isotropic turbulence) and its derivative.

The concomitant anisotropy in the temperature field accelerates the decay of temperature fluctuations.

INTRODUCTION

Significant measurements of the effects of gross strain upon homogeneous turbulence have been made by Townsend (ref. 1) and Uberoi (refs. 2 and 3). Townsend ran grid-produced turbulence through a nearly constant-area distortion in which the channel section went from a 4-to-1 rectangle to a 1-to-4 rectangle. The mean velocity was nearly constant. Uberoi ran grid-produced turbulence through a square channel contraction, which was essentially an axially symmetric distortion. He tested with contraction ratios of 4 to 1, 9 to 1, and 16 to 1.

They both made measurements of the three components of turbulent kinetic energy, the mean-square derivatives (giving the values of dissipation scales), as well as of the pertinent turbulent energy spectra before and after distortion.

Their principal results may be qualitatively summarized as follows:

(a) Distortion of roughly isotropic turbulence increases the velocities associated with the vorticity components which amplify by vortex line stretching. This phenomenon was predicted and estimated by Prandtl (ref. 4).

(b) The gross strain destroys isotropy not only of the energy-bearing eddies but also of the turbulent fine structure. There was departure from "local isotropy" in the distorting part of the channels.

(c) The longitudinal and lateral spectra are deformed somewhat as predicted by the calculations of Ribner and Tucker (ref. 5) and Batchelor and Proudman (ref. 6).

(d) Neither arrangement corresponded to a "rapid" distortion. There was appreciable transfer of energy among turbulence components during the straining process.

(e) In a straight channel following the distorting section, the return to local isotropy is fairly rapid, but the return to general isotropy is relatively slow.

Direct theoretical work on this problem began with Prandtl who used models consisting of steady, inviscid-stream tubes and vortex tubes (ref. 4). This work was followed by the cellular vortex analysis of Taylor (ref. 7), which is the basis for the more recent work. Ribner and Tucker (ref. 5) and Batchelor and Proudman (ref. 6) independently applied Taylor's model more realistically by simple Fourier synthesis. This most recent theory assumes (1) instantaneous distortion, so there is no decay or intercomponent transfer during distortion, and (2) homogeneous distortion. Ribner and Tucker appended a semiempirical correction to include decay when the distortion is not instantaneous. Using the same model, Acharya recently calculated some details of the case in which the unstrained field is axisymmetric (ref. 8).

The present investigation was undertaken to confirm and extend the Townsend-Uberoi findings on turbulence dynamics. In addition, a roughly isotropic (scalar) field of small temperature fluctuations was added to the turbulence so that the effect of gross distortion upon homogeneous turbulent mixing could be studied. Explicit predictions on the relative structure of scalar and velocity fields have been given chiefly in the isotropic case (refs. 9 to 11), although some exploratory analysis has also been directed at the axisymmetric case (refs. 12 and 13). Experimental study of this homogeneous mixing problem has been confined to the nearly isotropic fields behind a warm grid (refs. 14 and 15).

It has long been known that in the absence of shear stresses anisotropic turbulence will tend to become isotropic at sufficiently large Reynolds numbers. For example, the turbulence generated by a regular grid in a uniform stream reaches a fairly homogeneous but somewhat axisymmetric state by perhaps 30 mesh lengths downstream (refs. 16 and 17). This tends to become isotropic farther downstream. Townsend and Uberoi found this tendency in their postdistortion fields. Remarkably, the theoretical studies of homogeneous axisymmetric turbulence (refs. 18 to 20 and 12) have still produced no prediction of the rate at which this occurs. Therefore, it seemed desirable to make some detailed measurements at the downstream end of the channel for comparison with the immediate postcontraction turbulence.

This work was carried out at the Johns Hopkins University under the sponsorship and with the financial support of the National Advisory Committee for Aeronautics. The authors would like to thank Dr. L. S. G. Kovasznay, Dr. R. Betchov, Dr. F. H. Clauser, Mr. L. T. Miller, and Dr. D. W. Dunn of the Aeronautics Department of the Johns Hopkins University for their helpful interest and Mr. S. Bhaduri for his careful preparation of the figures.

SYMBOLS

| | |
|------------|--|
| a | hot-wire sensitivity |
| c | mean velocity ratio (hence streamwise distortion), \bar{U}_2/\bar{U}_1 (when used as a variable, $c(x) \equiv \bar{U}(x)/\bar{U}_1$) |
| E | one-dimensional energy spectrum (subscript indicates field variable) |
| e_1, e_2 | voltage fluctuations across two hot wires |
| f, g | principal two-point velocity correlations in isotropic turbulence |
| K | two-point velocity triple-correlation coefficient of u , $\frac{\overline{u_1^2 u_2}}{\overline{u_1^2} \overline{u_2}}$ |
| k | wave number in x-direction |
| L | integral scale of random field (subscript indicates field variable), \int_0^∞ (Correlation function)dr |

| | |
|--|---|
| M | grid mesh size |
| m | two-point temperature double-correlation coefficient, $\overline{\theta_1 \theta_2} / \theta_1' \theta_2'$ |
| n | two-point temperature triple-correlation coefficient, $\overline{\theta_1^2 \theta_2} / \theta_1'^2 \theta_2'$ |
| m,n | indices |
| p | static pressure |
| Q | two-point velocity double-correlation-coefficient functions |
| q | resultant fluctuation velocity, $\sqrt{u^2 + v^2 + w^2}$ |
| r | scalar distance between two observation points |
| S, S _u , S _θ | skewness factors for $\frac{\partial u}{\partial x}$, u, and θ, respectively |
| t | time |
| $\bar{U}, \bar{V}, \bar{W}$ | mean velocity components along x, y, and z axes |
| u, v, w | velocity fluctuation components along x, y, and z axes, respectively |
| x, y, z | Cartesian coordinates |
| x _i , x _j , x _k | Cartesian coordinates, tensor notation |
| α ₂ | angle between tunnel axis and line joining deflection points in section downstream of contraction |
| β | angle measured around tunnel axis |
| γ | thermal diffusivity |
| η | coordinate difference in y-direction |
| $\bar{\theta}$ | mean temperature rise across grid |
| θ | temperature fluctuation |
| λ | dissipative scale of random field (subscript indicates field variable) |

| | |
|-------------------|--|
| ν | kinematic viscosity |
| ξ | coordinate difference in x-direction |
| ρ | fluid density |
| $\overline{(\)}$ | average value |
| $(\)'$ | root-mean-square value, $\sqrt{\overline{(\)^2}}$ |

Subscripts:

| | |
|---------------|---|
| ax | axisymmetric |
| f,g | refer to f and g correlations, respectively |
| i,j,k | tensor notation referring to x-, y-, and z-directions, respectively |
| iso | value for isotropic (undistorted) field at equal time |
| l,m,n | indices |
| o | reference value |
| u,v, θ | refer to u, v, and θ , respectively |
| 1,2 | upstream and downstream of contraction, respectively |
| | parallel to tunnel axis |
| \perp | perpendicular to tunnel axis |

EXPERIMENTAL ARRANGEMENT

The basic wind tunnel was the open-return unit sketched in reference 9. The only addition was a secondary contraction with 4-to-1 velocity ratio starting $19\frac{3}{8}$ inches downstream of the grid (fig. 1). After the contraction was an almost uniform channel, slightly divergent to maintain constant static pressure (hence constant velocity) in spite of boundary-layer growth. This channel permitted some study of the history of the axisymmetric turbulence emerging from the contraction.

The measured mean-velocity distribution of the tunnel is shown in figure 2. The free-stream velocity fluctuation levels upstream of the grid were $\frac{u'}{\bar{U}} \approx 0.08$ percent and $\frac{v'}{\bar{U}} = \frac{w'}{\bar{U}} \approx 0.1$ percent. An appreciable part of this was pulsation resulting from the unbalance inevitable in the low-quality centrifugal fan used to move the air. The relative excess energy in lateral fluctuations is, of course, characteristic of wind tunnels with contractions and is consistent with the behavior of the contracted grid turbulence which is the primary subject of this study.

The biplane, square-mesh, fluctuation-generating grid was of 1/4-inch-diameter, round metal rods (Calrod heating units) set 1 inch on centers. It was heated with 60-cycle, 220-volt, 3-phase alternating current, and had sufficient thermal inertia that no 120-cycle periodic temperature fluctuations could be detected downstream.

A principal difficulty to be overcome was a "built-in" vertical mean-temperature gradient characteristic of the wind-tunnel-plus-room system. Individual current controls on the horizontal rods permitted reducing this to a difference of 0.2° C over the height of the tunnel working section. Figure 8 of reference 15 shows this, as well as a typical horizontal distribution of mean temperature, which was uniform to within $\pm 0.05^\circ$ C. The mean-temperature rise through the grid $\bar{\theta}$ was 5° C at a wind speed of 14 feet per second.

Both velocity and temperature fluctuations were reasonably homogeneous over the tunnel cross section at some distance behind the grid. Typical traverses of root-mean-square temperature θ' and velocity u' fluctuations before and after contraction are given in figures 3(a) and 3(b). The two sets of points in figure 3(b) were run at different times.

The negligibility of the effect of air-density fluctuations upon the turbulence dynamics was confirmed by the equality of turbulence levels and velocity correlation functions with and without heating.

MEASURING EQUIPMENT

Velocity and temperature fluctuations were both measured with a hot-wire anemometer (ref. 21). The basic equipment is described in reference 22. The auxiliary circuitry for squaring, cubing, etc. is described in reference 15.

Because of the extremely small temperature fluctuations to be detected, unusually high-resistance hot-wires (between 75 and 150 ohms) were used. These were of 0.00005-inch-diameter platinum (Wollaston)

about 0.1 inch long. No length corrections have been applied to the data, but the high wire resistance necessitated correction for current fluctuations in this nominally constant current equipment.

EXPERIMENTAL PROCEDURES

The experimental procedures used here were largely the same as those described in reference 15. The only additional variables were the lateral velocity fluctuations v and w . These were detected in standard fashion by the difference voltage of a (directionally sensitive) \times -meter.

Power spectra of u , v , and θ were determined with the aid of a Hewlett-Packard 300-A wave analyzer. All double correlations as well as the isotropic precontraction triple correlations were obtained as in reference 15, but the postcontraction triple correlations of u

required a bit more elaborate procedure in regions where $\overline{u^3} \neq 0$. The extra effect can be schematically shown by assuming linearized and identical wire response, compensated for thermal lag, so that the two output voltage fluctuations due to velocity are

$$\left. \begin{aligned} e_1 &= -au(x,y,z,t) \\ e_2 &= -au(x+\xi,y+\eta,z,t) \end{aligned} \right\} \quad (1)$$

Then

$$6a^3 \overline{u^2(x,y,z,t)u(x+\xi,y+\eta,z,t)} = \overline{(e_1 - e_2)^3} - \overline{(e_1 + e_2)^3} + 2\overline{e_2^3} \quad (2)$$

In true isotropic or axisymmetric turbulence, $\overline{u^3}$ must be zero, so $\overline{e_2^3}$ is also zero within the approximation of linear wire response.

In practice, of course, equation (2) was not used directly but was corrected for (a) unequal sensitivities of the two wires and (b) non-linearity of wire response, as outlined in the appendix of reference 15.

An attempt was made to determine the triple correlations

$\overline{\theta^2(x,y,z,t)\theta(x+\xi,y+\eta,z,t)}$ and $\overline{u(x,y,z,t)\theta(x,y,z,t)\theta(x+\xi,y+\eta,z,t)}$, but the combination of small thermal signals and complex triple-correlation

computation procedure yielded excessive scatter in the data, especially for the latter quantity.

EXPERIMENTAL RESULTS

Figure 4 demonstrates that the velocity and temperature fields are both axisymmetric after the contraction. This shows double-correlation values measured with two wires separated by a fixed radius in the same yz plane ($\alpha_2 = 90^\circ$). One wire was fixed on the tunnel axis, and the other was rotated to a series of positions on a circle about the axis. The value of r is the radius of this circle.

Figure 5(a) gives local turbulence levels along the tunnel axis. It was found that $w' \approx v'$, so only v' data were taken extensively. A more dramatic indication of the amplification of lateral fluctuations is given by numbers proportional to the root-mean-square fluctuations themselves, as in figure 5(b).

For comparing the histories of strained and unstrained turbulence, time rather than distance is obviously the appropriate reference. The conversion curve from x/M to a dimensionless time $t\bar{U}_1/M$ is given in figure 6. Figure 7(a) shows the first such comparison, the square root of the total turbulent energy ($\approx q' \equiv \sqrt{\overline{u^2} + \overline{v^2} + \overline{w^2}}$). The unstrained results here, as in several other figures, are taken from reference 15. These results are sometimes called isotropic. The data on root-mean-square temperature fluctuation (fig. 7(b)) are contrasted with the unstrained case in figure 7(c). Evidently the distortion hastens decay.

A class of important statistical point functions of turbulence is the "skewness factor" of any variable. This is a dimensionless measure of the third moment of the probability density and is central in that it may be a measure of nonlinear effects. In isotropic turbulence, the velocity fluctuations themselves must have zero skewness because of the required invariance to coordinate reflection; for example,

$$S_u \equiv \frac{\overline{u^3}}{(\overline{u^2})^{3/2}} = 0$$

This condition is well met by grid-generated turbulence. However, isotropy does not require that velocity-component derivatives in the direction of the components $\partial u/\partial x$, $\partial v/\partial y$, and $\partial w/\partial z$ have zero skewness.

One of the quantitative challenges to any isotropic theory is the prediction of the generally measured value of about -0.4 for quantities such as

$$S \equiv \frac{\overline{\left(\frac{\partial u}{\partial x}\right)^3}}{\left[\overline{\left(\frac{\partial u}{\partial x}\right)^2}\right]^{3/2}}$$

Figures 8(a) and 8(b) show the considerable effect of the contraction on these two skewness factors. Figure 8(c) summarizes the data on a time scale.

The small discrepancy between S in the unstrained field just ahead of contraction and S at the same station without later contraction (ref. 15) is probably a chance inconsistency between sets of data taken some weeks apart and at slightly different locations in the cross section of the duct.

The return to isotropic values by both S_u and S is evidently more rapid than the return of v'/u' .

A condition of isotropy in a scalar field like θ does not require that θ have statistical symmetry. Nevertheless, it was found in the unstrained case (ref. 15) that S_θ approaches zero rapidly. Figures 8(d) and 8(e) show that although the strained θ approaches zero skewness later in space, it actually goes down faster in time.

The temperature-gradient fluctuation, being a vector, must be statistically symmetrical in an isotropic field, and an attempt was made to measure the skewness of $\partial\theta/\partial x$ along the axis of the duct. Unfortunately, differentiation with respect to time $\left(\frac{\partial\theta}{\partial x} \approx \frac{1}{\bar{U}} \frac{\partial\theta}{\partial t}\right)$ decreased the signal-to-noise ratio too much for reliable measurement.

The effect of contraction on the energy spectra of longitudinal and lateral velocity fluctuations is at least qualitatively detectable in figures 9(a) and 9(b). The abscissae of the postcontraction curves are $\frac{\bar{U}_2}{\bar{U}_1} k$ instead of k so that the simple geometrical distortion effect is removed. Relatively, then, it is clear that the strain has favored the

small structure in u and the large structure in v . This is consistent with previous work, both experimental and theoretical.

The temperature spectra, similarly compared (fig. 9(c)), show less difference. This means that the contraction has acted primarily as a geometrical distortion of the scalar field.

Double- and triple-correlation functions downstream of the contraction at $x/M = 45$ and 73 (fig. 10) provide a fairly detailed picture of the nature of the distorted fields and their subsequent development. The precontraction correlations at $x/M = 17$ are given in figures 17(b), 19(b), 21(a), and 22(a) of reference 15.

The double correlations of u and θ are each given for three different values of α_2 , the angle between the tunnel axis and the line joining the detection points. The v -correlations were measured at only two angles. Comparison of figures 10(a) and 10(b) shows a decided trend toward isotropy in the straight duct following the contraction.

Typical two-point velocity triple-correlation functions in the post-contraction turbulence (figs. 10(g) and 10(h)) also show a trend toward isotropy. Inadequate signal-to-noise ratio led to excessive scatter in the attempts to measure the temperature triple correlations. Still, the general character for three different directions after distortion at $x/M = 45$ can be gleaned from figure 10(i). The corresponding precontraction data (nearly isotropic, at $x/M = 17$) are in figure 25 of reference 15.

"Integral scales" are defined from velocity double-correlation functions. At a given (nominal) value of x :

$$\left. \begin{aligned} L_{||}(\alpha_2) &\equiv \int_0^{\infty} Q_{||}(r, \alpha_2) \, dr \\ L_{\perp}(\alpha_2) &\equiv \int_0^{\infty} Q_{\perp}(r, \alpha_2) \, dr \end{aligned} \right\} \quad (3)$$

In figure 11(a) these are compared with the isotropic integral scales,

$$\left. \begin{aligned} L_f &\equiv \int_0^{\infty} f(r) \, dr \\ L_g &\equiv \int_0^{\infty} g(r) \, dr \end{aligned} \right\} \quad (4)$$

where, in isotropic turbulence,

$$\left. \begin{aligned} Q_{||}(r, 0^\circ) &= Q_{\perp}(r, 90^\circ) = f(r) \\ Q_{\perp}(r, 0^\circ) &= Q_{||}(r, 90^\circ) = g(r) \end{aligned} \right\} \quad (5)$$

Therefore, in figure 11(a), $L_{||}(5^\circ)$ and $L_{\perp}(90^\circ)$ have departed from the L_f curve. There is not enough information in the figure to tell even roughly when these integral scales will reach their isotropic relative values.

The same is true of the thermal integral scales (fig. 11(b)). In this case, however, the rough spectral similarity maintained through the contraction (fig. 9(c)) suggests that one look for a corresponding proportional distortion of the values of L_θ : at $\frac{t\bar{U}_1}{M} = 27$, $\frac{L_\theta(5^\circ)}{L_{\theta iso}} \approx 3$ and $\frac{L_\theta(90^\circ)}{L_{\theta iso}} \approx 0.6$. For simple instantaneous affine distortion these values would be 4 and 0.5, respectively.

Some of the dissipative scales have been obtained graphically from double-correlation functions. They are the abscissa intercepts of the vertex-osculating parabolas:

$$\left. \begin{aligned} \frac{1}{\lambda_{||}^2(\alpha_2)} &\equiv -\frac{1}{2} \left[\frac{\partial^2}{\partial r^2} Q_{||}(r, \alpha_2) \right]_{r=0} \\ \frac{1}{\lambda_{\perp}^2(\alpha_2)} &\equiv -\frac{1}{2} \left[\frac{\partial^2}{\partial r^2} Q_{\perp}(r, \alpha_2) \right]_{r=0} \\ \frac{1}{\lambda_\theta^2(\alpha_2)} &\equiv -\frac{1}{2} \left[\frac{\partial^2}{\partial r^2} m(r, \alpha_2) \right]_{r=0} \end{aligned} \right\} \quad (6)$$

The values of $\lambda_{||}$ and λ_{\perp} are compared with the undistorted dissipative scales in figure 12(a). These isotropic values are taken from reference 15:

$$\left. \begin{aligned} -\frac{1}{\lambda_f^2} &\equiv \frac{1}{2} \left(\frac{\partial^2 f}{\partial r^2} \right)_{r=0} \\ -\frac{1}{\lambda_g^2} &\equiv \frac{1}{2} \left(\frac{\partial^2 g}{\partial r^2} \right)_{r=0} \end{aligned} \right\} \quad (7)$$

Here $\lambda_{||}(5^\circ)$ and $\lambda_{\perp}(90^\circ)$ are departures from λ_f ; $\lambda_{||}(90^\circ)$ and $\lambda_{\perp}(5^\circ)$ are departures from λ_g . As with the integral scales, not all of these quantities appear to return rapidly to their isotropic relative values. However, the more extensive data on mean-square velocity derivatives (also related to the values of λ) taken by Townsend and Uberoi do show a strong return to isotropy. The evidence in figure 12(a) must be regarded as simply inadequate to permit any independent conclusion.

The values of λ_θ at $\frac{t\bar{U}_1}{M} = 27$ (fig. 12(b)) are moderately consistent with interpretation in terms of simple geometrical distortion through the contraction: $\frac{\lambda_\theta(5^\circ)}{\lambda_{\theta_{iso}}} \approx 4.1$ and $\frac{\lambda_\theta(90^\circ)}{\lambda_{\theta_{iso}}} \approx 0.7$. In the interval from $\frac{t\bar{U}_1}{M} = 27$ to $\frac{t\bar{U}_1}{M} = 34$ there is no appreciable return toward isotropy in the λ_θ values.

Figure 13 is a rough estimate, from the data, of the relative decay rates of temperature and velocity fluctuations. In the unstrained case (dashed line, from ref. 15) this quantity appears to approach an asymptote of 0.6.

TURBULENCE LEVELS

The behavior of v'/u' in a contraction is qualitatively given by Prandtl's theory of differential vortex stretching (ref. 4). For a quantitative theoretical prediction one can turn to the Ribner-Tucker analysis (ref. 5). Values obtained by this analysis, including a semiempirical estimate of energy decay from isotropic data, compare with those in figure 5(b) as follows:

| Ratio | Ribner-Tucker method | Measured |
|-----------------------------------|----------------------|----------|
| u_2'/u_1' | 0.4 | 0.7 |
| v_2'/v_1' | 1.5 | 1.4 |
| $\frac{(v_2'/u_2')}{(v_1'/u_1')}$ | 3.8 | 2.0 |

Only the v' prediction appears to be satisfactory, but even this conclusion must be tempered by the likelihood that there is appreciable transfer of energy from v' and w' to u' during the straining process. Such an effect could account for the particularly low u_2' estimated by the Ribner-Tucker method. On the basis of total turbulent energy, the agreement is good:

| Ratio | Ribner-Tucker method | Measured |
|-------------|----------------------|----------|
| q_2'/q_1' | 1.2 | 1.2 |

It was concluded that the gross strain rate inflicted on the turbulence field was far from rapid, a conclusion also reached by Townsend and by Uberoi for their experiments. Both the energy decay and the intercomponent transfer were appreciable during the 0.033-second-contraction transit time. A characteristic decay time is λ_g/u' , which was about 0.025 second just entering the contraction. For a rapid strain, the transit time would have to be much less than this.

There is still insufficient axisymmetric turbulence theory to define a time characterizing its rate of approach to isotropy, for example, an intercomponent-energy transfer time. If, however, this is an inertial effect (acting through the pressure-velocity correlations), L_g/u' might be a plausible choice. This was 0.044 second entering the contraction.

The foregoing paragraphs raise the question of whether it is feasible to produce rapid contraction of turbulence in the laboratory. For example, the contraction nozzle used in the present tests probably could not be shortened by more than a factor of 2 without inducing boundary-layer separation immediately upstream or downstream. But even halving the transit time would not make it negligible compared with λ_g/u' or L_g/u' .

Foregoing the assumption of instantaneous distortion, the downstream development of the turbulence can be displayed by means of Reynolds' turbulent-energy equations.

For the three component energies,

$$\frac{1}{2} \bar{U}_k \frac{\partial \overline{u^2}}{\partial x_k} = -\bar{u}_i \bar{u} \frac{\partial \bar{U}}{\partial x_i} - \frac{1}{2} \frac{\partial}{\partial x_j} (\overline{u_j u^2}) - \frac{1}{\rho} \bar{u} \frac{\partial p}{\partial x} + \overline{v u \nabla^2 u} \quad (8)$$

$$\frac{1}{2} \bar{U}_k \frac{\partial \overline{v^2}}{\partial x_k} = -\bar{u}_i \bar{v} \frac{\partial \bar{V}}{\partial x_i} - \frac{1}{2} \frac{\partial}{\partial x_j} (\overline{u_j v^2}) - \frac{1}{\rho} \bar{v} \frac{\partial p}{\partial y} + \overline{v v \nabla^2 v} \quad (9)$$

$$\frac{1}{2} \bar{U}_k \frac{\partial \overline{w^2}}{\partial x_k} = -\bar{u}_i \bar{w} \frac{\partial \bar{W}}{\partial x_i} - \frac{1}{2} \frac{\partial}{\partial x_j} (\overline{u_j w^2}) - \frac{1}{\rho} \bar{w} \frac{\partial p}{\partial z} + \overline{v w \nabla^2 w} \quad (10)$$

or, adding these,

$$\frac{1}{2} \bar{U}_k \frac{\partial \overline{q^2}}{\partial x_k} = -\overline{u_i u_m} \frac{\partial \bar{U}_m}{\partial x_i} - \frac{1}{2} \frac{\partial}{\partial x_j} (\overline{u_j q^2}) - \frac{1}{\rho} \frac{\partial}{\partial x_l} (\overline{u_l p}) + \overline{v u_n \nabla^2 u_n} \quad (11)$$

A first approximation, suitable for the present case, follows from the assumption that turbulent mean values are nearly constant in the yz plane, for example, that $\left| \frac{\partial \bar{u}^2}{\partial y} \right| \ll \left| \frac{\partial \bar{u}^2}{\partial x} \right|$. This also involves

$\left| \frac{\partial \bar{U}}{\partial y} \right| \ll \left| \frac{\partial \bar{U}}{\partial x} \right|$, although there is no such inequality for \bar{V} and \bar{W} . Then

$$\frac{1}{2} \bar{U} \frac{\partial \overline{u^2}}{\partial x} \approx -\bar{u}^2 \frac{\partial \bar{U}}{\partial x} - \frac{1}{2} \frac{\partial \overline{u^3}}{\partial x} - \frac{1}{\rho} \bar{u} \frac{\partial p}{\partial x} + \overline{v u \nabla^2 u} \quad (12)$$

$$\frac{1}{2} \bar{U} \frac{\partial \overline{v^2}}{\partial x} \approx -\bar{v}^2 \frac{\partial \bar{V}}{\partial y} - \frac{1}{2} \frac{\partial \overline{u v^2}}{\partial x} - \frac{1}{\rho} \bar{v} \frac{\partial p}{\partial y} + \overline{v v \nabla^2 v} \quad (13)$$

$$\frac{1}{2} \bar{U} \frac{\partial \overline{w^2}}{\partial x} \approx -\bar{w}^2 \frac{\partial \bar{W}}{\partial z} - \frac{1}{2} \frac{\partial \overline{u w^2}}{\partial x} - \frac{1}{\rho} \bar{w} \frac{\partial p}{\partial z} + \overline{v w \nabla^2 w} \quad (14)$$

In this approximation, it is also assumed that \overline{uv} , \overline{vw} , and \overline{wu} are negligible. Adding to get the total turbulent kinetic energy and using axial symmetry (e.g., $\overline{v^2} = \overline{w^2}$) as well as mean-flow continuity,

$$\frac{1}{2} \bar{U} \frac{\partial \overline{q^2}}{\partial x} \approx (\overline{v^2} - \overline{u^2}) \frac{\partial \bar{U}}{\partial x} - \frac{1}{2} \frac{\partial}{\partial x} (\overline{u^3} + 2\overline{uv^2}) - \frac{1}{\rho} \frac{\partial}{\partial x} \overline{up} + \overline{vu_j v^2 u_j} \quad (15)$$

A still rougher approximation follows from restricting to very small turbulence levels, so that one can expect inequalities like

$$\left| \frac{\partial \overline{u^3}}{\partial x} \right| \ll \bar{U} \left| \frac{\partial \overline{u^2}}{\partial x} \right| \quad (16)$$

If p' is of the order $\overline{pu^2}$, the static-pressure term can also be neglected:

$$\frac{1}{2} \bar{U} \frac{\partial \overline{u^2}}{\partial x} \approx -\overline{u^2} \frac{\partial \bar{U}}{\partial x} + \overline{vu^2 v} \quad (17)$$

Since $\overline{v^2} = \overline{w^2}$, add equations (13) and (14) and eliminate \bar{V} and \bar{W} in terms of \bar{U} :

$$\frac{1}{2} \bar{U} \frac{\partial \overline{v^2}}{\partial x} \approx \frac{1}{2} \overline{v^2} \frac{\partial \bar{U}}{\partial x} + \overline{vv^2 v} \quad (18)$$

Comparison of the first terms on the right-hand sides of equations (17) and (18) shows clearly that values of $\frac{\partial \bar{U}}{\partial x} > 0$ tend to decrease $\overline{u^2}$ and to increase $\overline{v^2}$ and $\overline{w^2}$.

The $\overline{q^2}$ equation simplifies to

$$\frac{1}{2} \bar{U} \frac{\partial \overline{q^2}}{\partial x} \approx (\overline{v^2} - \overline{u^2}) \frac{\partial \bar{U}}{\partial x} + \overline{vu_1 v^2 u_1} \quad (19)$$

Equations (17) and (18) cannot be used further without an estimate of the viscous terms. First, it is convenient to transform

$$\overline{u^2 v^2} = \frac{1}{2} \overline{v^2 u^2} - \overline{\frac{\partial u}{\partial x_k} \frac{\partial u}{\partial x_k}} \quad (20)$$

with corresponding forms for v , w , and u_j . Even in turbulent shear flows the first of these terms is usually negligible, and the second is a good approximation to the dissipation. Then equations (17) and (18) are

$$\frac{1}{2} \bar{U} \frac{\partial \overline{u^2}}{\partial x} \approx -\overline{u^2} \frac{\partial \bar{U}}{\partial x} - \overline{v \frac{\partial u}{\partial x_1} \frac{\partial u}{\partial x_1}} \quad (21)$$

$$\frac{1}{2} \bar{U} \frac{\partial \overline{v^2}}{\partial x} \approx \frac{1}{2} \overline{v^2} \frac{\partial \bar{U}}{\partial x} - \overline{v \frac{\partial v}{\partial x_j} \frac{\partial v}{\partial x_j}} \quad (22)$$

An estimate, very rough indeed, could now be made by assuming simple geometrical distortion to relate these viscous terms to those in unstrained turbulence at equal times. It is already well established, however, that the behavior of the velocity field under strain involves dynamics as well as kinematics. It seems more reasonable, therefore, to save the technique outlined for a more appropriate problem, that of the strained temperature field.

TEMPERATURE FLUCTUATIONS

Without mean-temperature gradients, fluid strain has no effect on the probability density of the θ -field. Hence it has no instantaneous effect on moments such as $\overline{\theta^2}$. The strain obviously changes the temperature-gradient field, however, and hence the rate of decay of $\overline{\theta^2}$.

In fact, it is just this kind of effect which enables turbulent motion (through its random strain field) to promote rapid molecular-scale mixing.

The crudest estimate of mean-strain-accelerated $\overline{\theta^2}$ decay (fig. 7(c)) can be made by assuming statistically homogeneous and uniform mean strain. Then the decay equation is (ref. 10)

$$\frac{d\overline{\theta^2}}{dt} = -2\gamma \overline{\frac{\partial \theta}{\partial x_1} \frac{\partial \theta}{\partial x_1}} \quad (23)$$

Suppose the field is instantaneously strained by a factor $c \left(= \frac{\bar{U}_2}{\bar{U}_1} \right)$ in the x-direction and $1/\sqrt{c}$ in the y- and z-directions. With an isotropic

field before distortion, $\overline{\left(\frac{\partial\theta}{\partial x}\right)^2} = \overline{\left(\frac{\partial\theta}{\partial y}\right)^2} = \overline{\left(\frac{\partial\theta}{\partial z}\right)^2}$, and the immediate postdistortion derivatives are

$$\left. \begin{aligned} \overline{\left(\frac{\partial\theta}{\partial x}\right)^2} &= \frac{1}{c^2} \overline{\left(\frac{\partial\theta}{\partial x}\right)^2} \\ \overline{\left(\frac{\partial\theta}{\partial y}\right)^2} &= \overline{\left(\frac{\partial\theta}{\partial z}\right)^2} = c \overline{\left(\frac{\partial\theta}{\partial x}\right)^2} \end{aligned} \right\} \quad (24)$$

The decay rate immediately after distortion is then

$$\frac{d\overline{\theta^2}}{dt} = -2\gamma \overline{\left(\frac{\partial\theta}{\partial x}\right)^2} \left(\frac{1}{c^2} + 2c\right) \quad (25)$$

Assuming the unstrained history $\overline{\theta_1^2}(t)$ is known, the relative decay rate is initially

$$\frac{d\overline{\theta^2}}{d\overline{\theta_1^2}} = \frac{1}{3} \left(\frac{1}{c^2} + 2c\right) \quad (26)$$

Rather than attempt to apply this instantaneous-distortion analysis to the experiments, it seems worthwhile to consider a more general approach.

A more reasonable estimate requires (a) using the general $\overline{\theta^2}$ equation without assuming homogeneity (ref. 23), and (b) including $c = c(x)$ where $c(x) = \overline{U}(x)/\overline{U}_1$. With constant mean temperature,

$$\frac{1}{2} \overline{U}_i \frac{\partial \overline{\theta^2}}{\partial x_i} = -\frac{1}{2} \frac{\partial}{\partial x_k} \left(\overline{u_k \theta^2} \right) + \gamma \overline{\theta \nabla^2 \theta} \quad (27)$$

With x the direction of largest gradients,

$$\frac{1}{2} \overline{U} \frac{\partial \overline{\theta^2}}{\partial x} \approx -\frac{1}{2} \frac{\partial}{\partial x} \left(\overline{u \theta^2} \right) + \gamma \overline{\theta \nabla^2 \theta} \quad (28)$$

and for very small turbulence level, the triple correlation term is neglected. Making use of a transformation like equation (20) and neglecting the second derivative term,

$$\bar{U} \frac{\partial \overline{\theta^2}}{\partial x} \approx -2\gamma \frac{\partial \theta}{\partial x_1} \frac{\partial \theta}{\partial x_1} \quad (29)$$

Finally, ignoring the differences between the diffusion-induced growth rate of λ_θ in strained and unstrained flows,

$$\left. \begin{aligned} \overline{\left(\frac{\partial \theta}{\partial x}\right)^2} &\approx \frac{2}{c^2} \frac{\overline{\theta^2}}{\lambda_{\theta_1}^2} \\ \overline{\left(\frac{\partial \theta}{\partial y}\right)^2} &= \overline{\left(\frac{\partial \theta}{\partial z}\right)^2} \approx 2c \frac{\overline{\theta^2}}{\lambda_{\theta_1}^2} \end{aligned} \right\} \quad (30)$$

where $c(x) = \frac{\bar{U}(x)}{\bar{U}_1}$ and λ_{θ_1} is the dissipative scale for the unstrained case at the same time.

With time t as the independent variable, $\frac{\partial}{\partial x} \approx \frac{1}{\bar{U}} \frac{d}{dt}$, and equation (29) becomes

$$\frac{d\overline{\theta^2}}{dt} \approx -4\gamma \frac{\overline{\theta^2}}{\lambda_{\theta_1}^2} \left(\frac{1}{c^2} + 2c \right) \quad (31)$$

With given values of $c(t)$ and $\lambda_{\theta_1}(t)$ this could be numerically integrated, but the latter can be eliminated by seeking only the ratio of $\overline{\theta^2}$ in the strained and isotropic cases.

In terms of time, equation (29) can be written for the isotropic case as

$$\frac{d\overline{\theta_1^2}}{dt} \approx -12\gamma \frac{\overline{\theta_1^2}}{\lambda_{\theta_1}^2} \quad (32)$$

From equations (31) and (32),

$$\frac{d}{dt} \left(\frac{\overline{\theta^2}}{\theta_i^2} \right) \approx - \frac{4\gamma}{\lambda_{\theta_i}^2} \left(\frac{\overline{\theta^2}}{\theta_i^2} \right) \left(\frac{1}{c^2} + 2c - 3 \right) \quad (33)$$

or

$$\log_e \left(\frac{\overline{\theta^2}}{\theta_i^2} \right) \approx -4\gamma \int_0^t \left(\frac{1}{c^2} + 2c - 3 \right) \frac{dt_1}{\lambda_{\theta_i}^2} \quad (34)$$

Numerical integration of equation (34) from $x/M = 15$ (where it starts to deviate from the unstrained curve) to $x/M = 35$ gives as theoretical estimate for the difference

$$\frac{\theta_i' - \theta'}{\theta'} \approx 0.15$$

But the experimental value, from figure 8(e), is

$$\frac{\theta_i' - \theta'}{\theta'} = 0.35$$

which is more than twice as large. The weakest link in the analysis is probably equation (30). Inclusion of the effect of increased $\overline{q^2}$ (which reduces dissipative scales by increasing turbulence Reynolds number) only increases the theoretical estimate to 0.19.

SKEWNESS AND INHOMOGENEITY

For turbulence dynamics, the principal results are the effects of contraction on the skewnesses of u and $\frac{\partial u}{\partial x}$ ($\approx \frac{1}{U} \frac{\partial u}{\partial t}$). The generation of S_u during the straining process, when its value was negligible upstream, is evidence that the strain is appreciably inhomogeneous. The statistical symmetry of a homogeneous strain would preclude the production of u^3 unless it were present at the start.

A good theoretical estimate of $\overline{u^3}(x)$ is made difficult to obtain by the lack of knowledge of pressure-field statistics. The equation for $\overline{u^3}$ is derived by multiplying the u-equation by u^2 and then averaging:

$$\begin{aligned} \frac{1}{3} \overline{U} \frac{\partial \overline{u^3}}{\partial x} + \frac{1}{3} \overline{V} \frac{\partial \overline{u^3}}{\partial y} + \frac{1}{3} \overline{W} \frac{\partial \overline{u^3}}{\partial z} + \overline{u^3} \frac{\partial \overline{U}}{\partial x} + \overline{u^2 v} \frac{\partial \overline{V}}{\partial y} + \overline{u^2 w} \frac{\partial \overline{W}}{\partial z} + \frac{1}{3} \frac{\partial \overline{u^4}}{\partial x} + \frac{1}{3} \frac{\partial \overline{u^3 v}}{\partial y} + \\ \frac{1}{3} \frac{\partial \overline{u^3 w}}{\partial z} - \overline{u^2} \frac{\partial \overline{u^2}}{\partial x} - \overline{u^2} \frac{\partial \overline{uv}}{\partial y} - \overline{u^2} \frac{\partial \overline{uw}}{\partial z} = -\frac{1}{\rho} \overline{u^2} \frac{\partial p}{\partial x} + \overline{vu^2 \nabla^2 u} \end{aligned} \quad (35)$$

For a first approximation, it may be reasonable to assume

$$\left. \begin{aligned} |\overline{V}| = |\overline{W}| \ll |\overline{U}| \\ \left| \frac{\partial \overline{u^3}}{\partial y} \right| = \left| \frac{\partial \overline{u^3}}{\partial z} \right| \ll \left| \frac{\partial \overline{u^3}}{\partial x} \right| \\ |\overline{u^2 v}| = |\overline{u^2 w}| \ll |\overline{u^3}| \\ |\overline{uv}| = |\overline{uw}| \ll |\overline{u^2}| \end{aligned} \right\} \quad (36)$$

Then equation (35) reduces to

$$\frac{1}{3} \overline{U} \frac{\partial \overline{u^3}}{\partial x} \approx -\overline{u^3} \frac{\partial \overline{U}}{\partial x} - \frac{1}{3} \frac{\partial \overline{u^4}}{\partial x} + \frac{1}{2} \frac{\partial (\overline{u^2})^2}{\partial x} - \frac{1}{\rho} \overline{u^2} \frac{\partial p}{\partial x} + \overline{vu^2 \nabla^2 u} \quad (37)$$

Restriction to a low turbulence level does not permit neglecting the $\overline{u^4}$ and $(\overline{u^2})^2$ terms relative to the $\overline{u^3} \overline{U}$ terms because $\overline{u^3}$ is initially zero while $\overline{u^4}$ and $\overline{u^2}$ are not. On the other hand, $u^2 \frac{\partial p}{\partial x}$ is zero in

isotropic turbulence. If it is assumed that $p' = O(\rho \overline{u^2})$, restriction to a small turbulence level permits neglecting the pressure-velocity

term. If, furthermore, $\overline{u^4}$ is estimated roughly in terms of $\overline{u^2}$ by taking the Gaussian equality $\overline{u^4} \approx 3(\overline{u^2})^2$, equation (36) becomes

$$\frac{1}{3} \overline{u} \frac{\partial \overline{u^3}}{\partial x} \approx -\overline{u^3} \frac{\partial \overline{u}}{\partial x} - \frac{1}{2} \frac{\partial (\overline{u^2})^2}{\partial x} + \overline{vu^2 \nabla^2 u} \quad (38)$$

Some qualitative confirmation of this form can be obtained by using it to predict the sign of $\overline{u^3}$ in the early stages of the straining process. If $\overline{u^3}$ is identically zero at the origin of x and the effect of viscous force is ignored, equation (38) predicts $\overline{u^3} > 0$ for small values of x . In the present experiments it turned out that $\overline{u^3} > 0$ for all values of x .

Doubtless some knowledge of the viscous term in equation (38),

$$\begin{aligned} \overline{u^2 \nabla^2 u} &= \frac{1}{3} \frac{\partial^2 \overline{u^3}}{\partial x_i \partial x_i} - \frac{\partial u}{\partial x_j} \frac{\partial u^2}{\partial x_j} \\ &\approx - \frac{\partial u}{\partial x_j} \frac{\partial u^2}{\partial x_j} \end{aligned} \quad (39)$$

would be required for an estimate of $\overline{u^3}(x)$. On the other hand, there may be less effect of viscosity on the dimensionless ratio $\frac{\overline{u^3}}{(\overline{u'})^3} \equiv S_u$. Furthermore, it is possible that $u^2 \frac{\partial p}{\partial x}$ in equation (36) may still be negligible for low enough turbulence levels: with distortion it departs from zero, but so does the term $\overline{u^3} \frac{\partial \overline{u}}{\partial x}$.

By chain differentiation,

$$\frac{\partial S_u}{\partial x} \equiv \frac{\partial}{\partial x} \left[\frac{\overline{u^3}}{(\overline{u^2})^{3/2}} \right] = \frac{1}{(\overline{u^2})^{3/2}} \frac{\partial \overline{u^3}}{\partial x} - \frac{3}{2} \frac{S_u}{\overline{u^2}} \frac{\partial \overline{u^2}}{\partial x} \quad (40)$$

Substituting from equations (17) and (38), less viscous terms, this becomes

$$\frac{\partial S_u}{\partial x} \approx 6 \frac{u'}{\bar{U}^2} \frac{\partial \bar{U}}{\partial x} \quad (41)$$

Furthermore, u' can be expressed in terms of \bar{U} by integrating the inviscid form of equation (17)

$$u'(x) \approx \frac{\bar{U}_1}{\bar{U}(x)} u_1' \quad (42)$$

so that

$$\frac{\partial S_u}{\partial x} \approx 6 \bar{U}_1 u_1' \frac{1}{\bar{U}^3} \frac{\partial \bar{U}}{\partial x} \quad (43)$$

Therefore

$$S_u(x) \approx 3 \frac{u_1'}{\bar{U}_1} \left(1 - \frac{\bar{U}_1^2}{\bar{U}^2(x)} \right) \quad (44)$$

Entering the contraction, $\frac{u_1'}{\bar{U}_1} \approx 0.025$. At the end, $\bar{U}/\bar{U}_1 = 4$, so equation (43) predicts that $S_u \approx 0.07$ at the end; the measured value is about 0.075.

It is clear that this good agreement must be in part fortuitous. For example, in the straight section following the contraction equation (43) predicts a constant value of $S_u \approx 0.07$. Yet, in fact, S_u returns rather rapidly to zero. It has long been known that the inter-component energy transfer (accompanying a trend toward isotropy in homogeneous turbulence) depends upon pressure-velocity correlations which were neglected in this analysis.

CONCLUDING REMARKS

Measurements of the turbulence levels of grid-produced turbulence passing through a 4-to-1 contraction and a downstream straight duct agree with the results of Uberoi. They confirm in general the conclusions of both Townsend and Uberoi that reasonably smooth channel distortions cannot be regarded as sudden in terms of ordinary grid turbulence structure.

In addition, the relatively strong effects of this contraction on skewnesses of both the longitudinal velocity fluctuation and its derivative indicate that the contraction cannot even be regarded as homogeneous.

Establishment of this contraction as a rather slow and inhomogeneous distortion of this turbulence reduces the incentive for carrying out a detailed comparison of the correlation functions with predictions of a Ribner-Tucker-Batchelor-Proudman type of analysis. Nevertheless, the homogeneous, instantaneous approach accompanied by correction for dissipation does seem to give a satisfactory estimate for total turbulent-energy change.

The effect of a contraction in increasing the root-mean-square velocity fluctuation components v' and w' relative to u' suggests that nearly isotropic turbulence behind a grid (where v' and w' are less than u') may be obtained by a suitably small amount of contraction prior to the straight duct. (Uberoi reported in a private communication that he has tried this and found a strong tendency for the turbulence in the straight section to return to its axisymmetric state.)

The accelerated temperature-fluctuation decay due to strain is qualitatively understandable. The failure of the present (noninstantaneous) simple geometrical theory certainly indicates the need for a more detailed look at the problem.

Mechanical Engineering Department,
The Johns Hopkins University,
Baltimore, Md., March 23, 1958.

REFERENCES

1. Townsend, A. A.: The Uniform Distortion of Homogeneous Turbulence. Quart. Jour. Mech. and Appl. Math., vol. VII, pt. 1, Mar. 1954, pp. 104-127.
2. Uberoi, Mahinder S.: The Effect of Wind-Tunnel Contraction on Free-Stream Turbulence. Jour. Aero. Sci., vol. 23, no. 8, Aug. 1956, pp. 754-764.
3. Uberoi, Mahinder S.: Equipartition of Energy and Local Isotropy in Turbulent Flows. Jour. Appl. Phys., vol. 28, no. 10, Oct. 1957, pp. 1165-1170.
4. Prandtl, L.: Attaining a Steady Air Stream in Wind Tunnels. NACA TM 726, 1933.
5. Ribner, H. S., and Tucker, M.: Spectrum of Turbulence in a Contracting Stream. NACA Rep. 1113, 1953. (Supersedes NACA TN 2606.)
6. Batchelor, G. K., and Proudman, I.: The Effect of Rapid Distortion of a Fluid in Turbulent Motion. Quart. Jour. Mech. and Appl. Math., vol. VII, pt. 1, Mar. 1954, pp. 83-103.
7. Taylor, G. I.: Turbulence in a Contracting Stream. Z.a.M.M., Bd. 15, Heft 1, Feb. 1935, pp. 91-96.
8. Acharya, Y. V. G.: Spectrum of Axisymmetric Turbulence in a Contracting Stream. Proc. Ind. Acad. Sci., sec. A, vol. 44, no. 2, 1956, pp. 63-71.
9. Obukhoff, A. M.: Structure of the Temperature Field in Turbulent Flow. Bull., Acad. Sci. (USSR), Geofiz. Ser., vol. 13, no. 1, 1949, pp. 58-69.
10. Corrsin, Stanley: The Decay of Isotropic Temperature Fluctuations in an Isotropic Turbulence. Jour. Aero. Sci., vol. 18, no. 6, June 1951, pp. 417-423.
11. Corrsin, S.: On The Spectrum of Isotropic Temperature Fluctuations in an Isotropic Turbulence. Jour. Appl. Phys., vol. 22, no. 4, Apr. 1951, pp. 469-473.
12. Mélése, G. B.: On Axisymmetric Turbulence and Scalar Fields. Ph.D. Thesis, The Johns Hopkins Univ., June 1954.
13. Dunn, D. W., and Reid, W. H.: Heat Transfer in Isotropic Turbulence During the Final Period of Decay. NACA TN 4186, 1958.

14. Kistler, A. L., O'Brien, V., and Corrsin, S.: Preliminary Measurements of Turbulence and Temperature Fluctuations Behind a Heated Grid. NACA RM 54D19, 1954.
15. Mills, R. R., Jr., Kistler, A. L., O'Brien, V., and Corrsin, S.: Turbulence and Temperature Fluctuations Behind a Heated Grid. NACA TN 4288, 1958.
16. Corrsin, S.: Decay of Turbulence Behind Three Similar Grids. A. E. Thesis, C.I.T., June 1942.
17. Grant, H. L., and Nisbet, I. C. T.: The Inhomogeneity of Grid Turbulence. Jour. Fluid Mech., vol. 2, pt. 3, May 1957, pp. 263-272.
18. Batchelor, G. K.: The Theory of Axisymmetric Turbulence. Proc. Roy. Soc. (London), ser. A, vol. 186, no. 1007, Sept. 24, 1946, pp. 480-502.
19. Chandrasekhar, S.: The Theory of Axisymmetric Turbulence. Phil. Trans. Roy. Soc. (London), ser. A, vol. 242, no. 855, Sept. 5, 1950, pp. 557-577.
20. Chandrasekhar, S.: The Decay of Axisymmetric Turbulence. Proc. Roy. Soc. (London), ser. A, vol. 203, no. 1074, Oct. 10, 1950, pp. 358-364.
21. Corrsin, Stanley: Extended Applications of the Hot-Wire Anemometer. NACA TN 1864, 1949.
22. Corrsin, Stanley, and Uberoi, Mahinder S.: Spectra and Diffusion in a Round Turbulent Jet. NACA Rep. 1040, 1951. (Supersedes NACA TN 2124.)
23. Corrsin, Stanley: Heat Transfer in Isotropic Turbulence. Jour. Appl. Phys., vol. 23, no. 1, Jan. 1952, pp. 113-118.

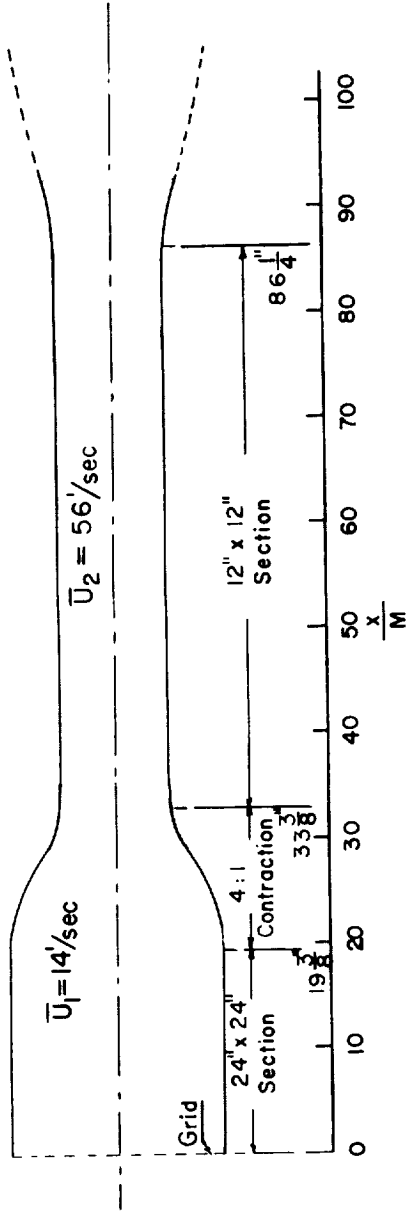


Figure 1.- Schematic sketch of wind tunnel.

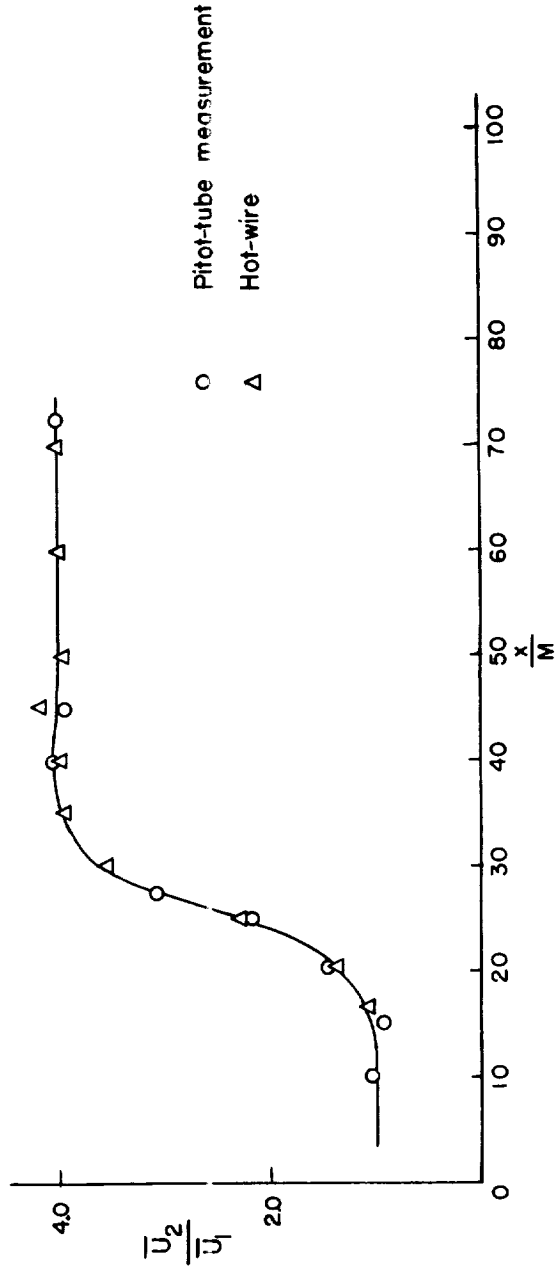
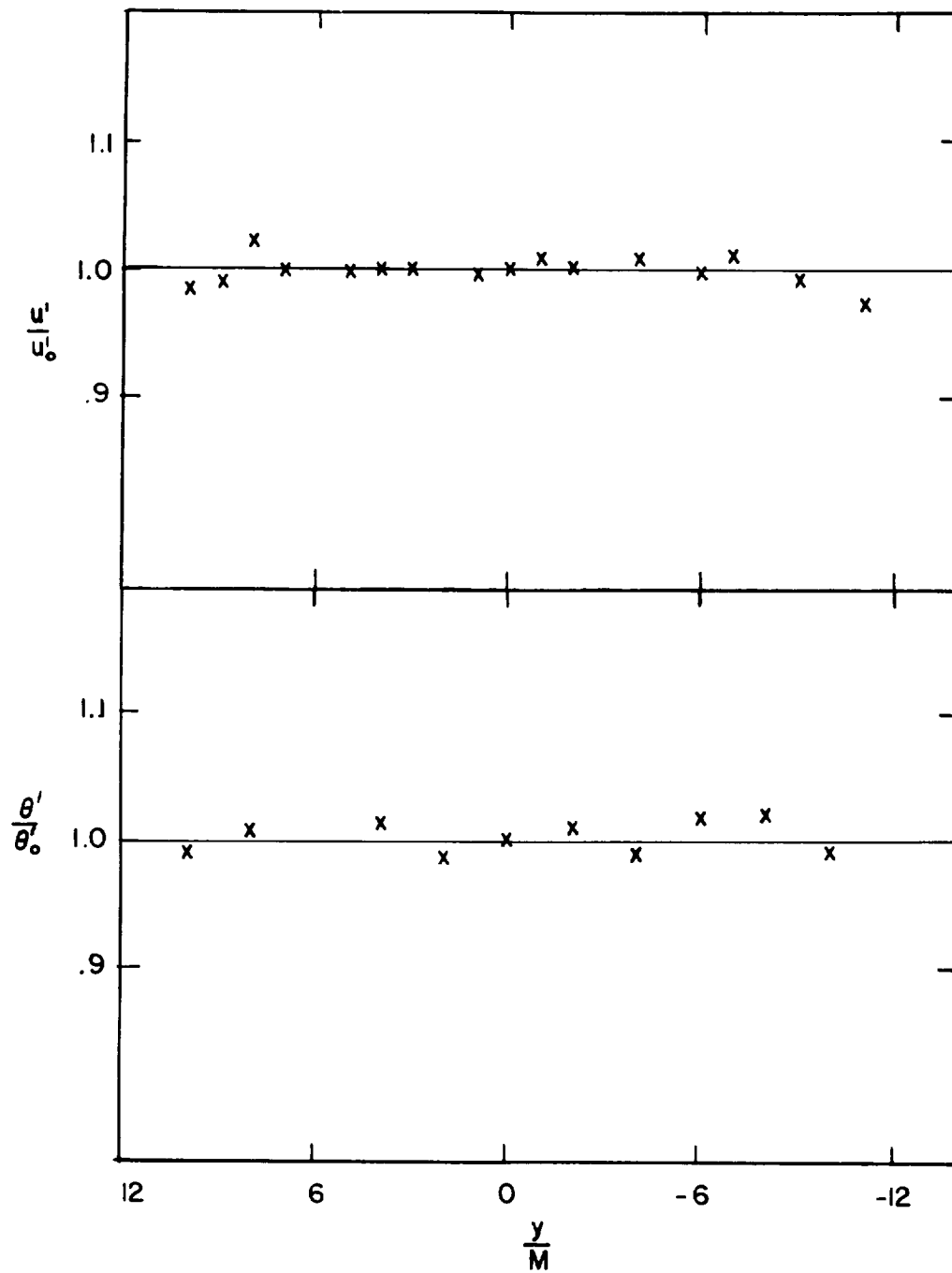
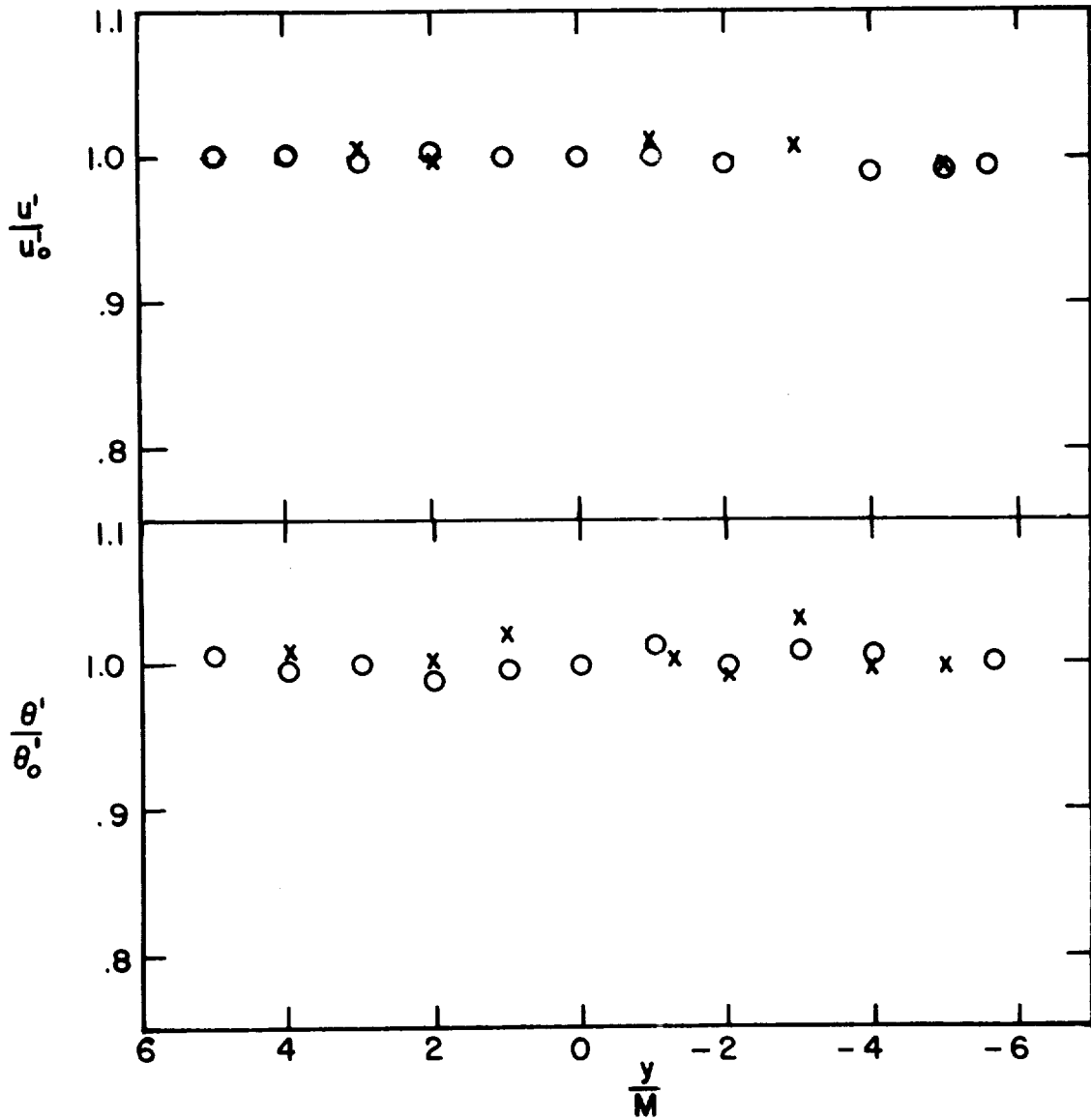


Figure 2.- Measured mean-velocity distribution of wind tunnel.



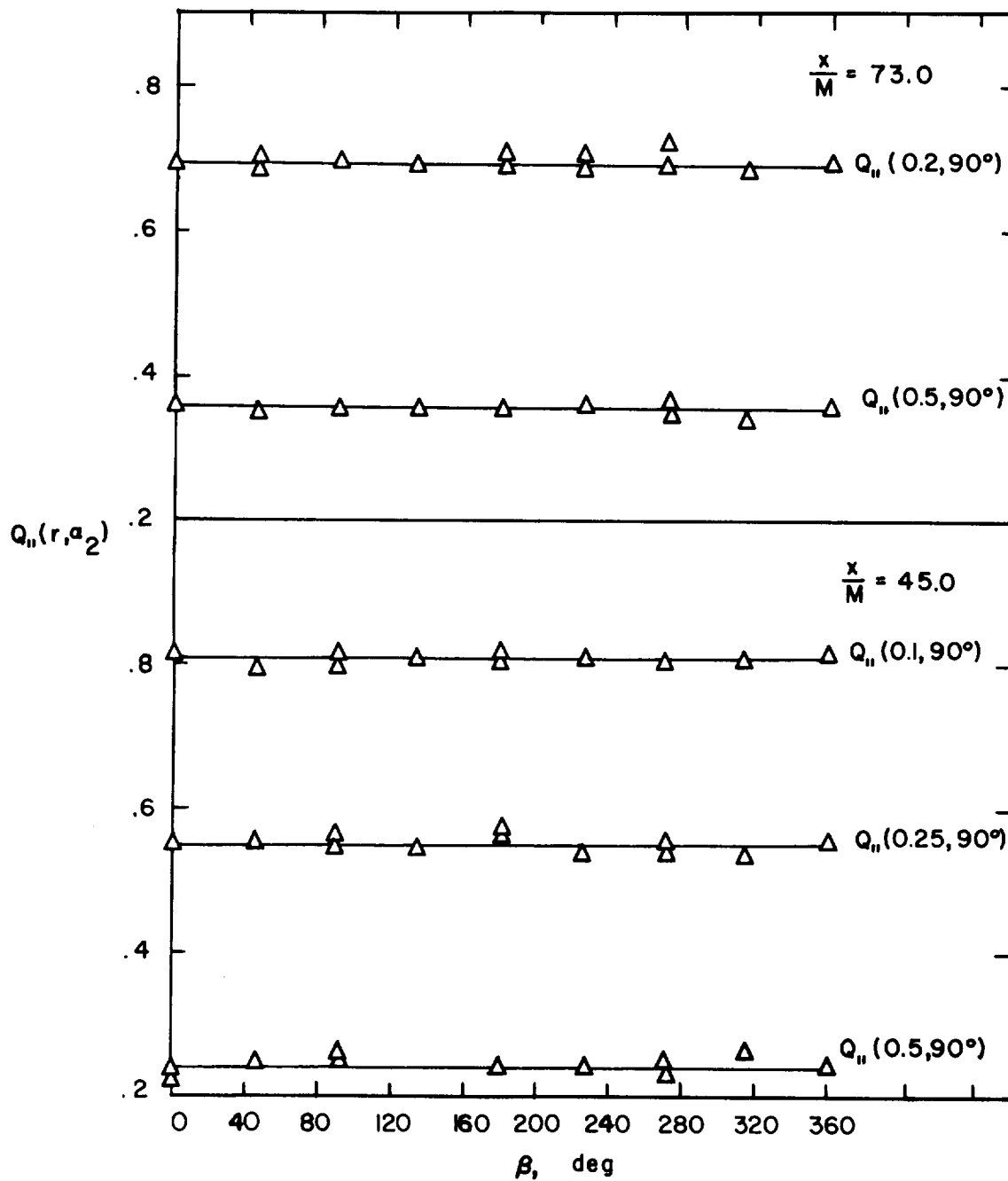
(a) Before contraction; $x/M = 17.0$.

Figure 3.- Typical traverses of root-mean-square temperature θ' and velocity u' fluctuations.



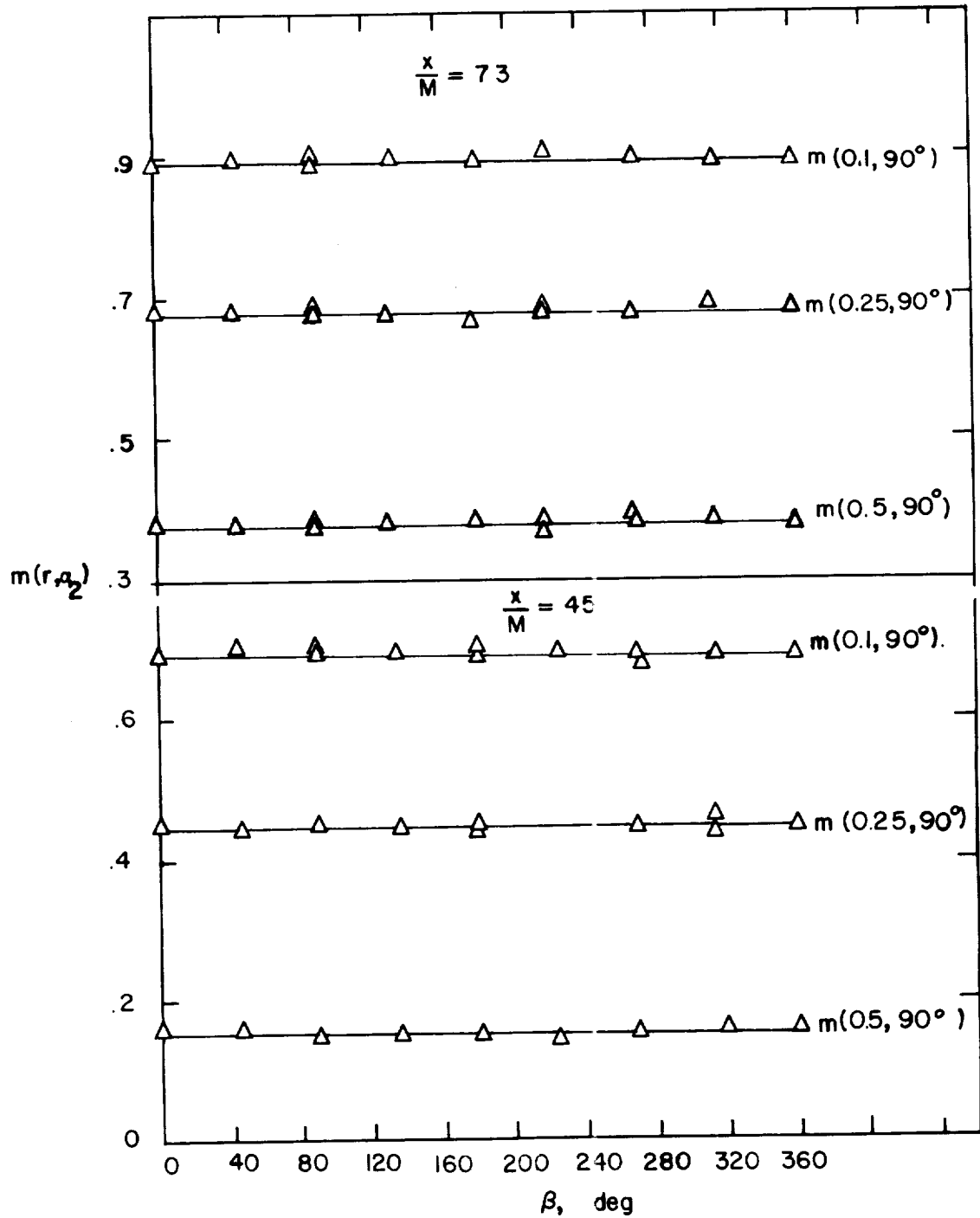
(b) After contraction; $x/M = 40$. Two sets of points denote data taken at different times.

Figure 3.- Concluded.



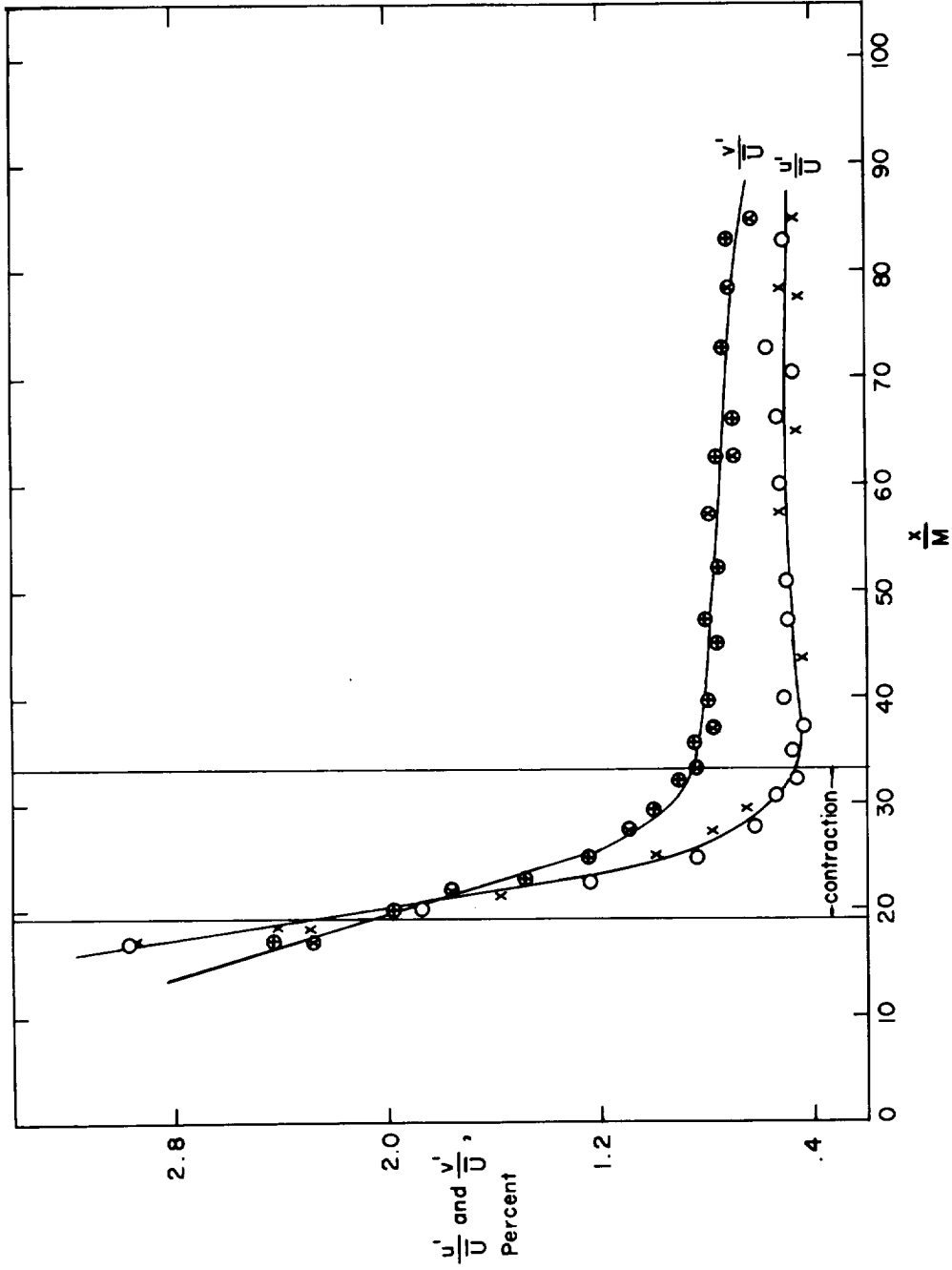
(a) Velocity field.

Figure 4.- Velocity and temperature fields after contraction.



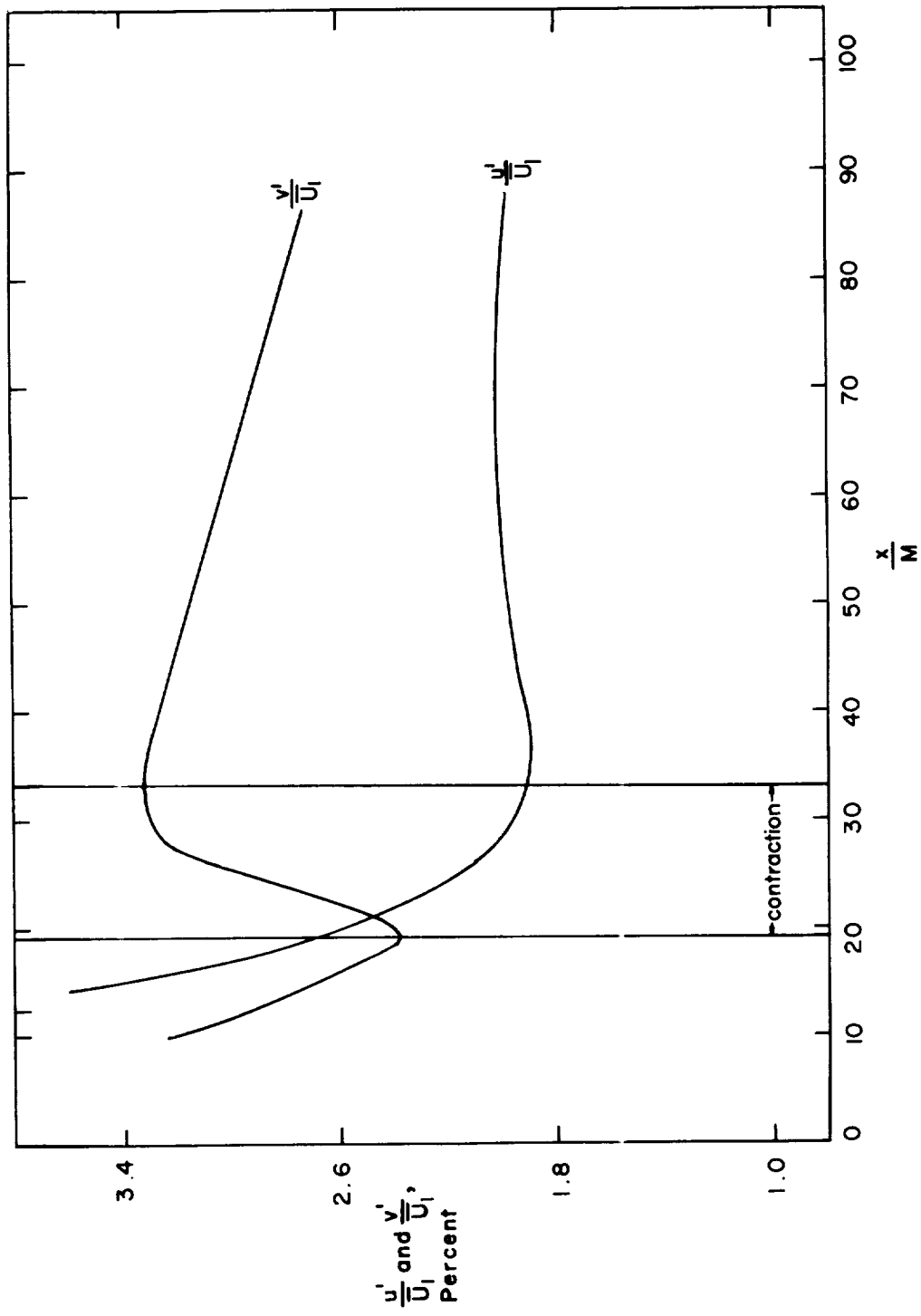
(b) Temperature field.

Figure 4.- Concluded.



(a) Sets of points on each curve denote data taken at different times.

Figure 5.- Longitudinal and lateral turbulence decay. $Re_M = 7420$.



(b) Curves drawn proportional to root-mean-square fluctuations.

Figure 5.- Concluded.

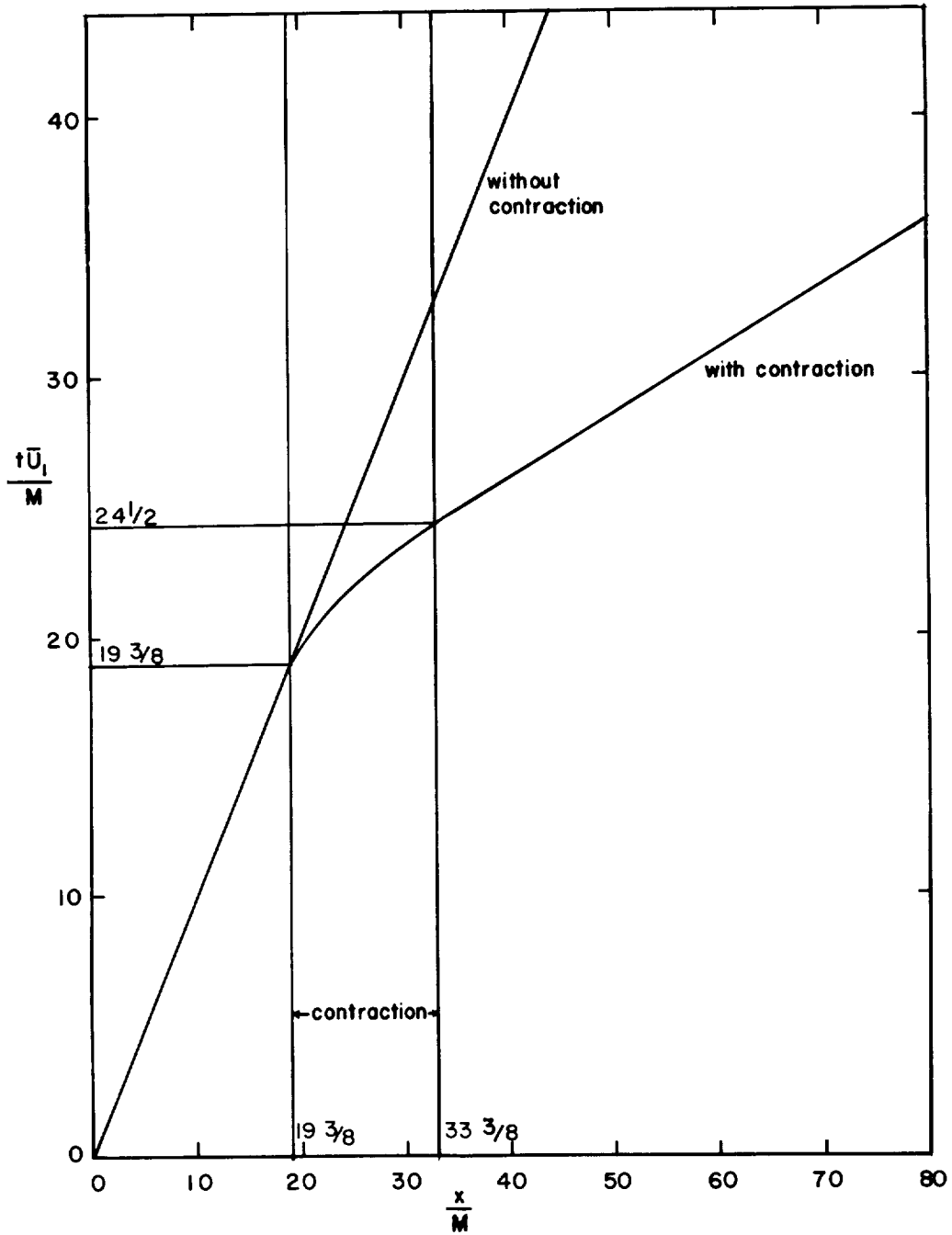
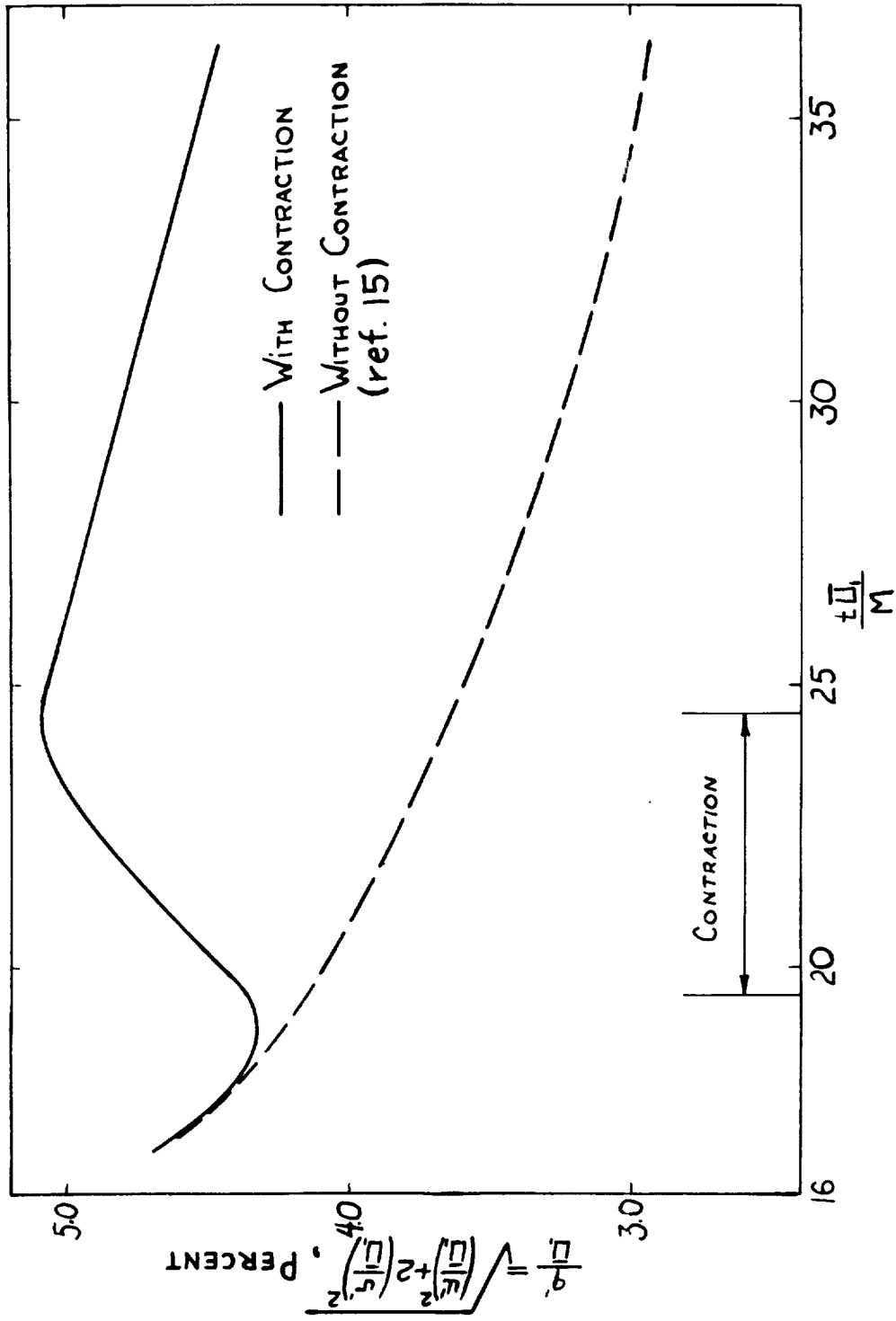


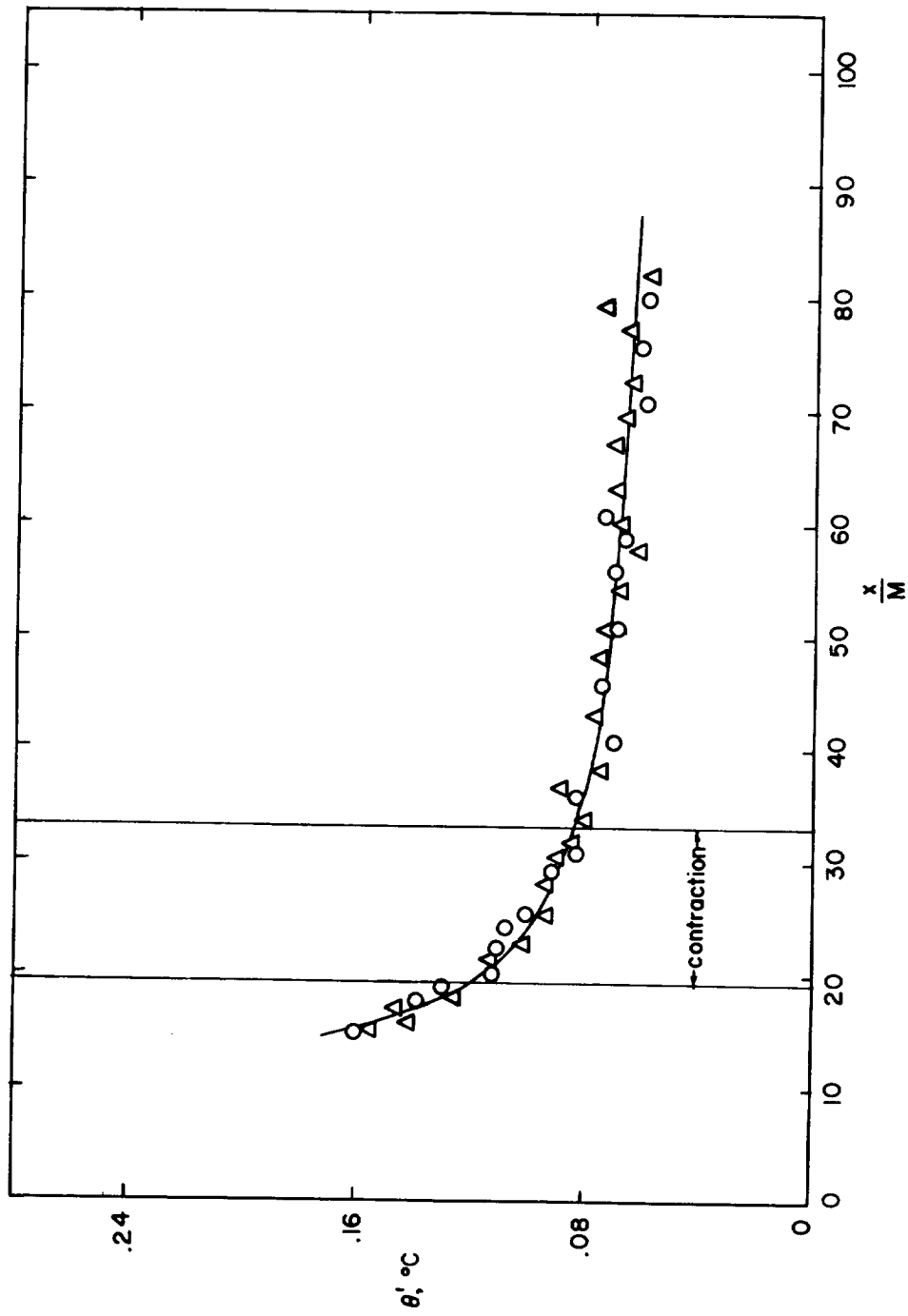
Figure 6.- Conversion curve from distance x/M to dimensionless

$$\text{time } \frac{t\bar{U}_1}{M}. \quad \frac{t\bar{U}_1}{M} \equiv \frac{U_1}{M} \int_0^x \frac{dx}{\bar{U}(x)}.$$



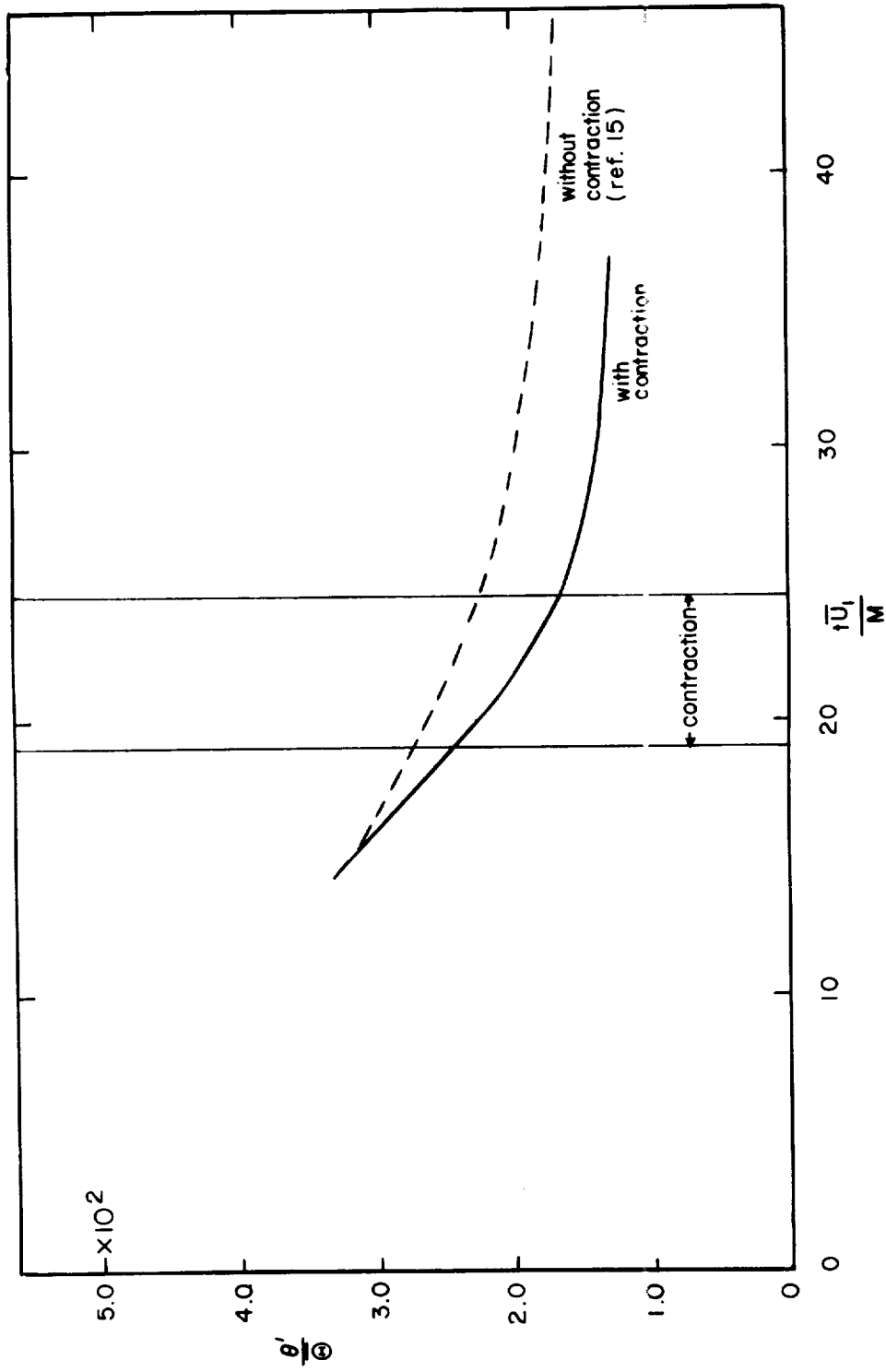
(a) Square root of total turbulent energy plotted against dimensionless time.

Figure 7.- Comparison of histories of strained and unstrained turbulence.



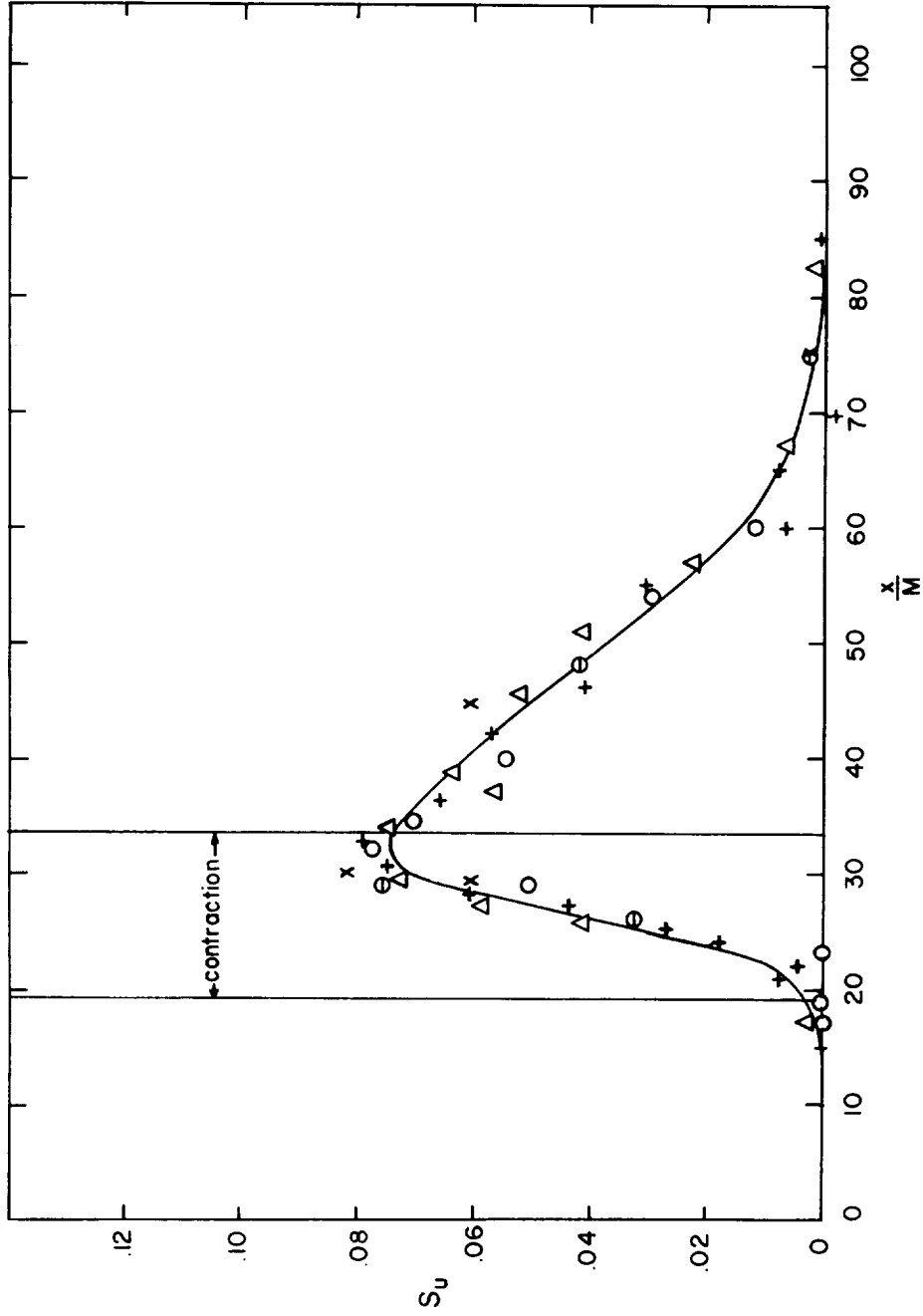
(b) Root-mean-square temperature fluctuation for strained turbulence.

Figure 7.- Continued.



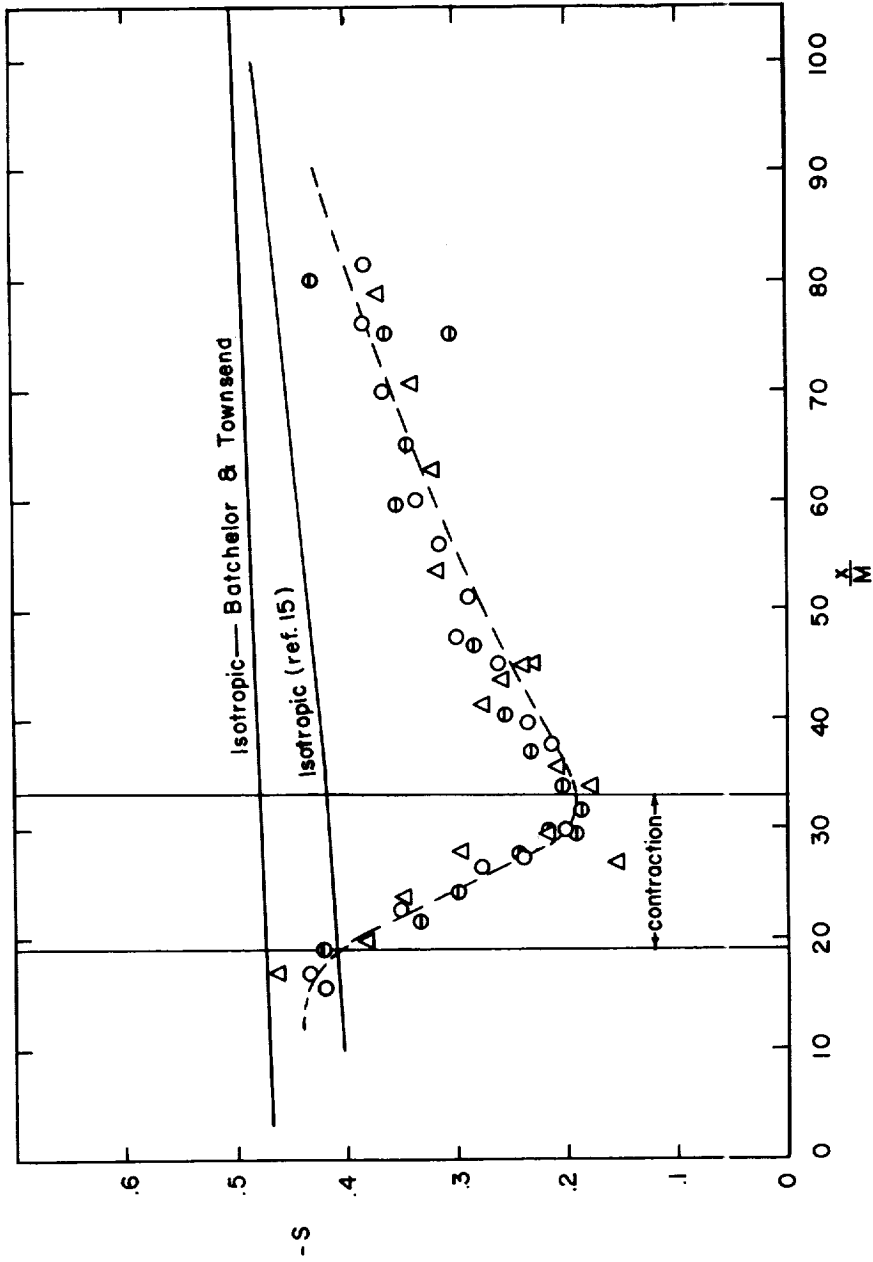
(c) Curve from figure 7(b) contrasted with curve for unstrained turbulence plotted against dimensionless time. $\theta = 5^\circ \text{C}$.

Figure 7.- Concluded.



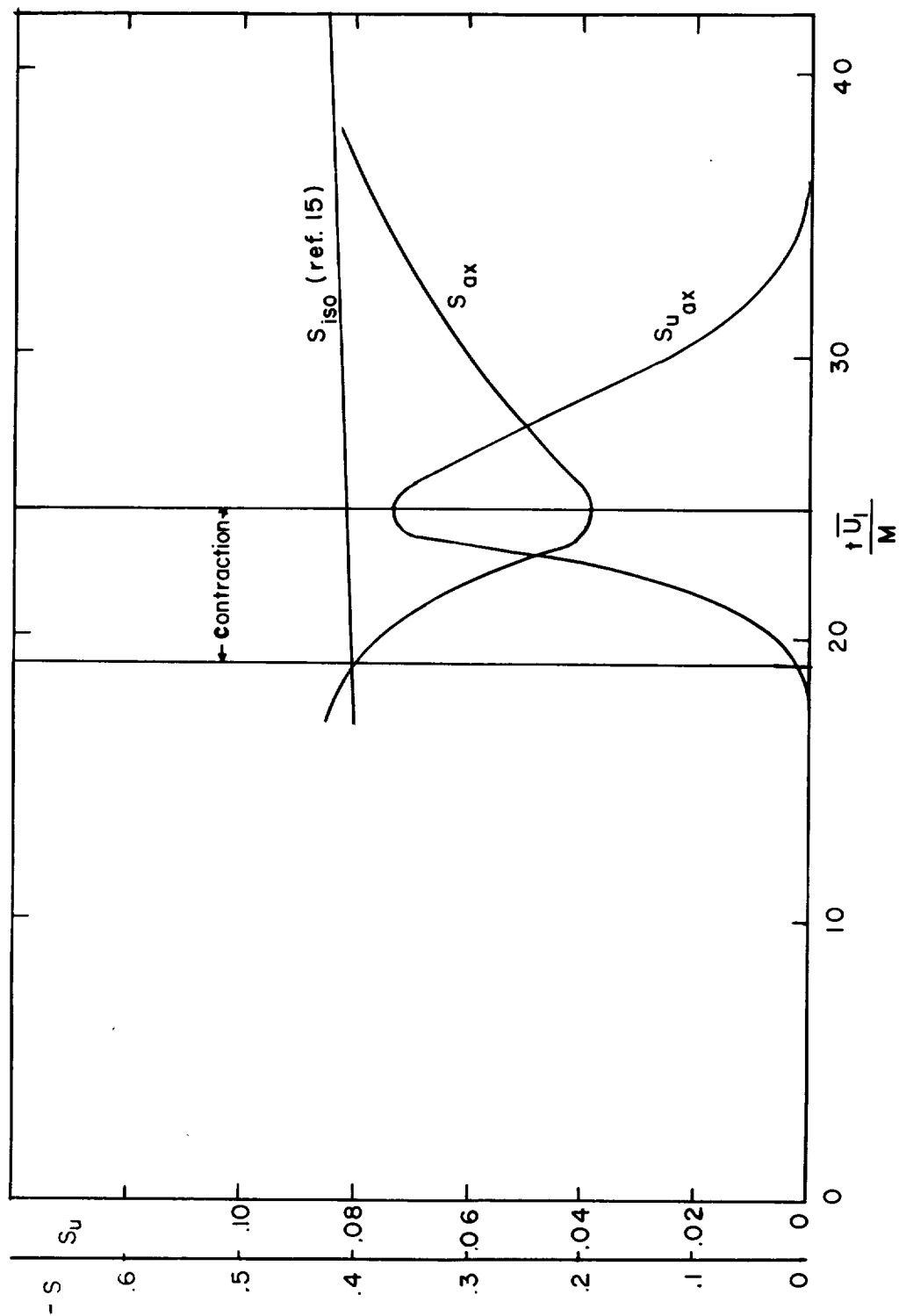
(a) Skewness factor for u plotted against distance; $S_u \equiv \frac{\overline{u^3}}{(\overline{u^2})^{3/2}}$.

Figure 8.- Effect of contraction on skewness factors. Different points indicate data taken at different times.



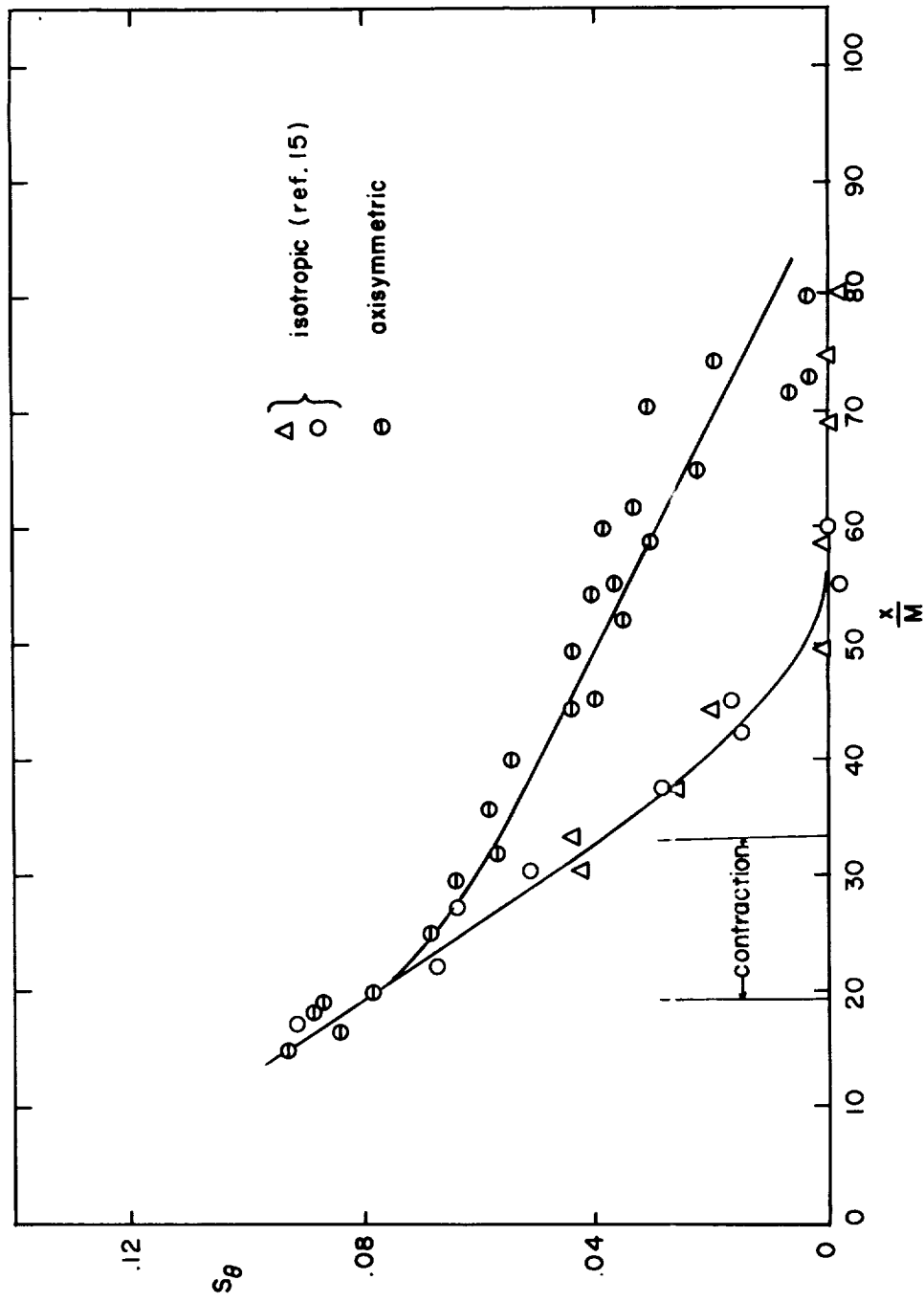
(b) Skewness factor for $\frac{\partial u}{\partial x}$ plotted against distance; $S = \frac{\overline{\left(\frac{\partial u}{\partial x}\right)^3}}{\left[\overline{\left(\frac{\partial u}{\partial x}\right)^2}\right]^{3/2}}$.

Figure 8.- Continued.



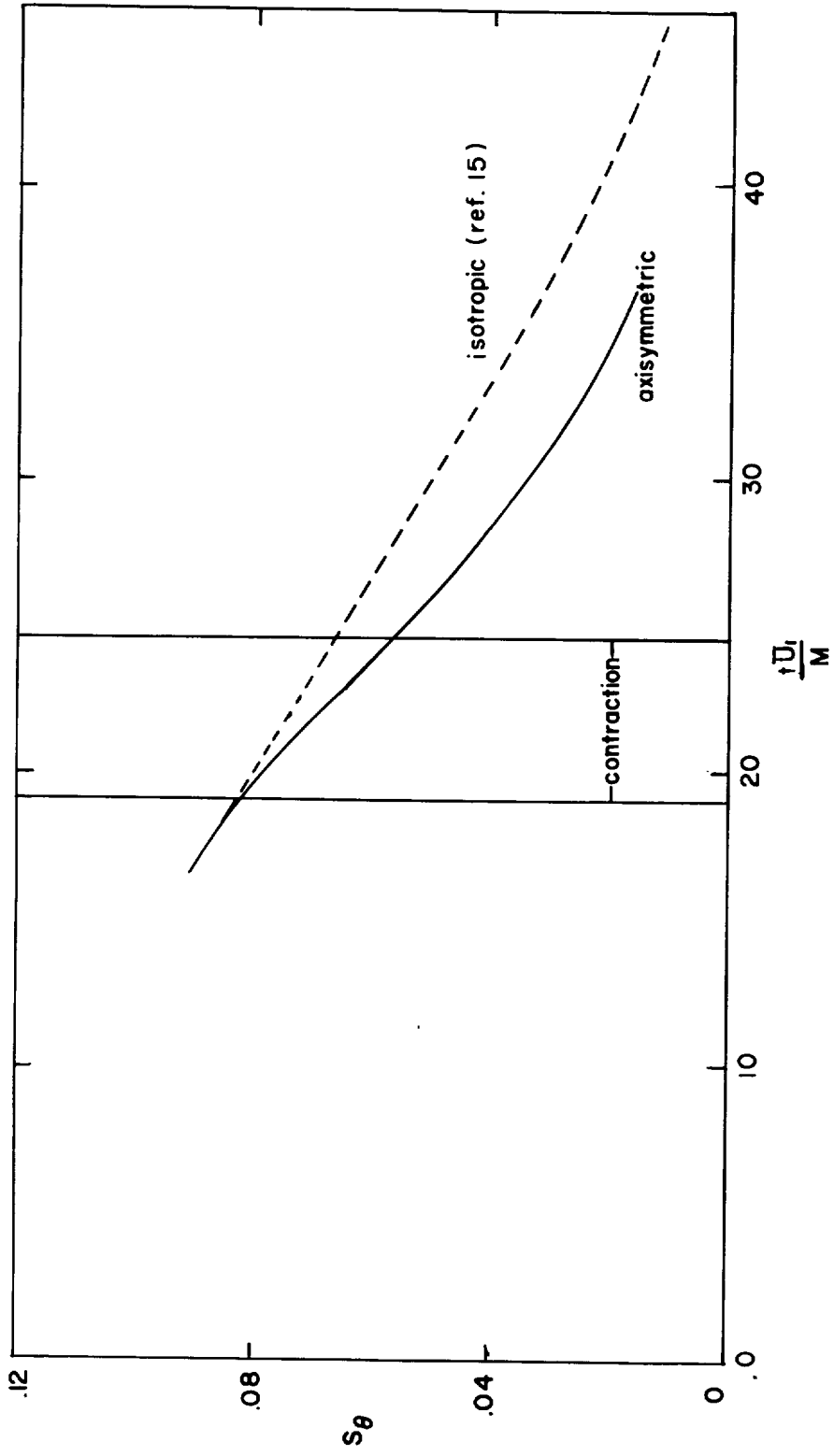
(c) Skewness factors for $\partial u/\partial x$ and u plotted against time.

Figure 8.- Continued.



(d) Skewness factor for time plotted against distance; $S_\theta = \frac{\overline{\theta^3}}{(\overline{\theta^2})^{3/2}}$.

Figure 8.- Continued.



(e) Skewness factor for time plotted against time.

Figure 8.- Concluded.

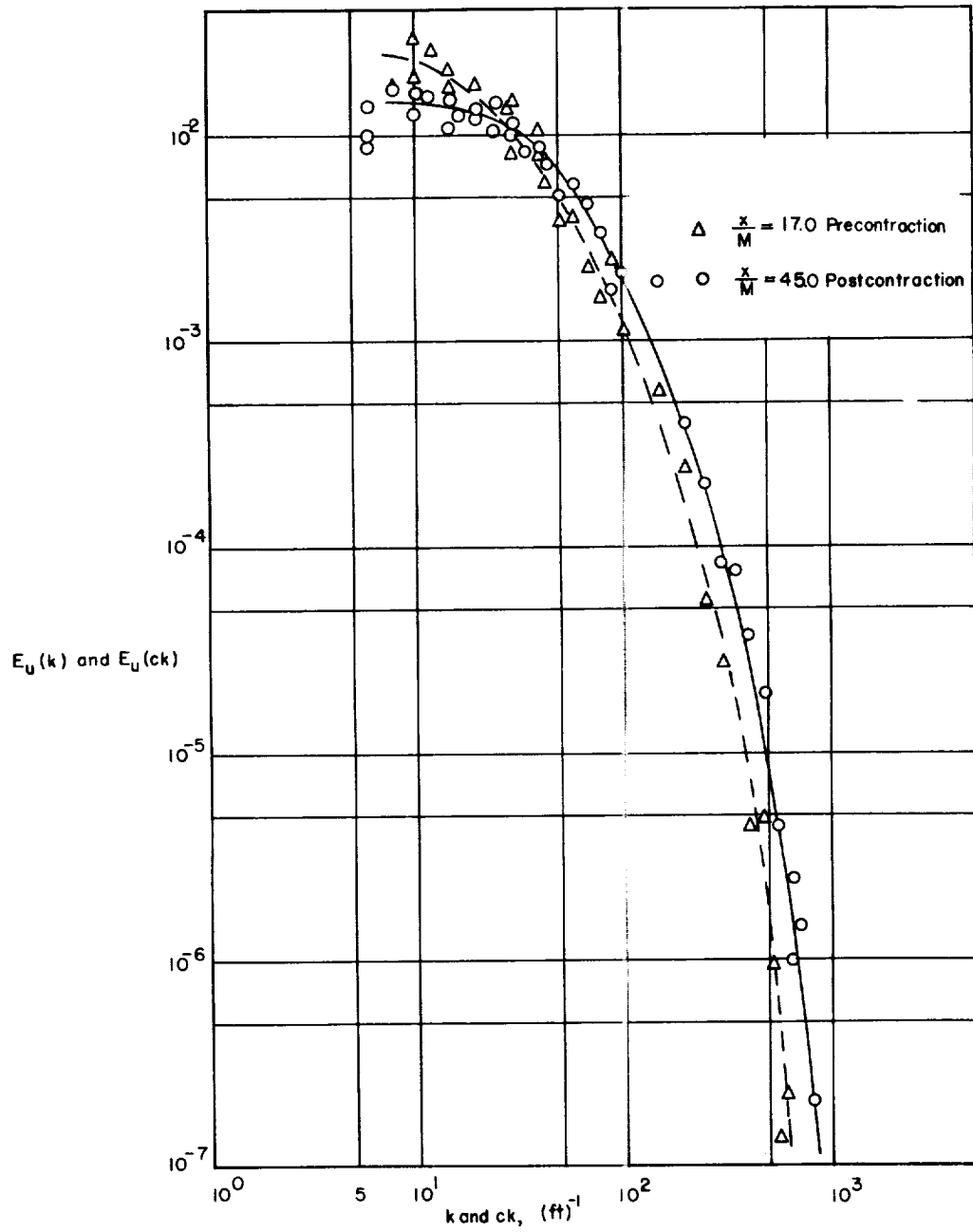
(a) Spectrum of $\overline{u^2}$.

Figure 9.- Effect of contraction on energy spectra of velocity fluctuations. $c = \frac{\overline{U_2}}{\overline{U_1}} = 4$.

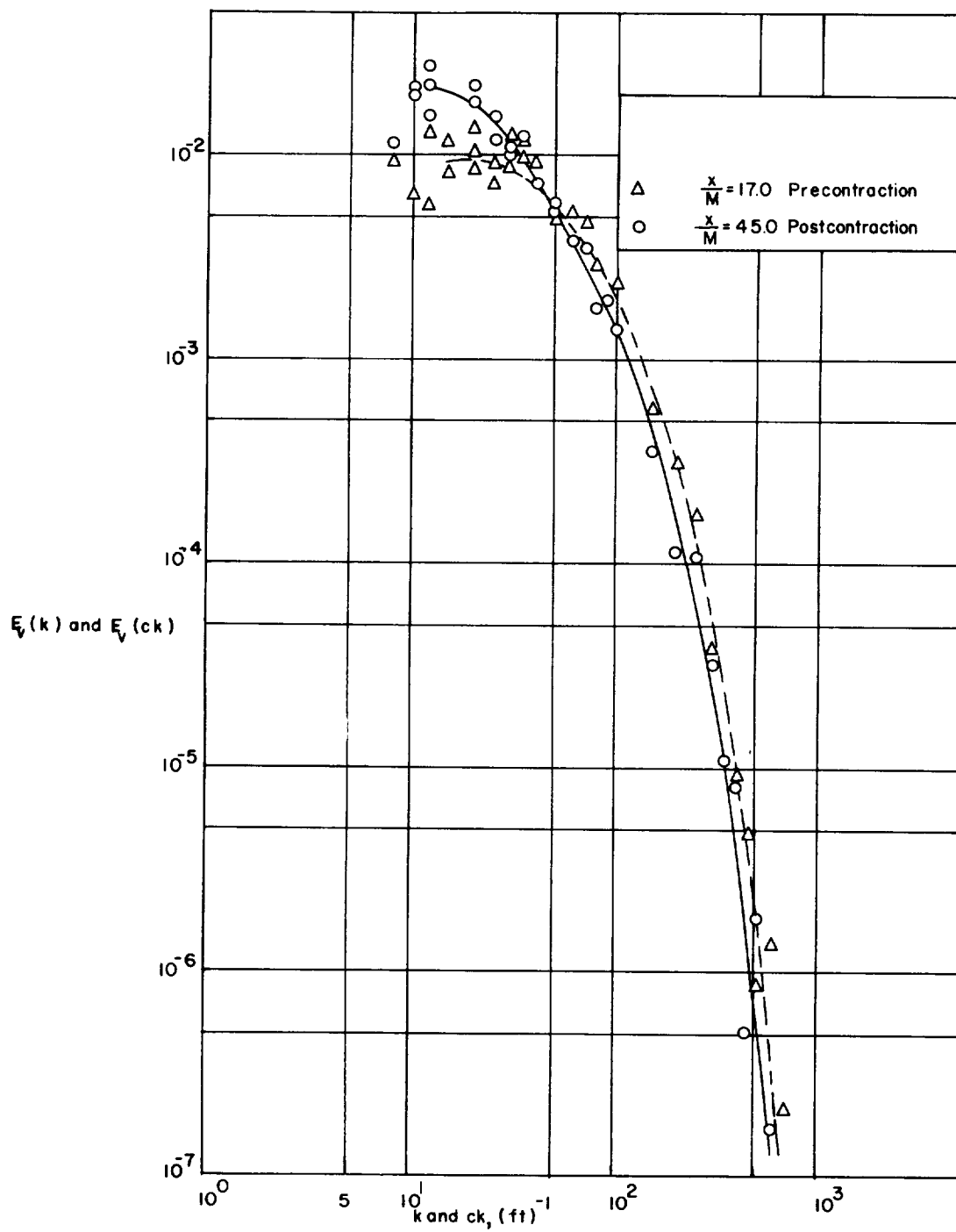
(b) Spectrum of $\overline{v^2}$.

Figure 9.- Continued.

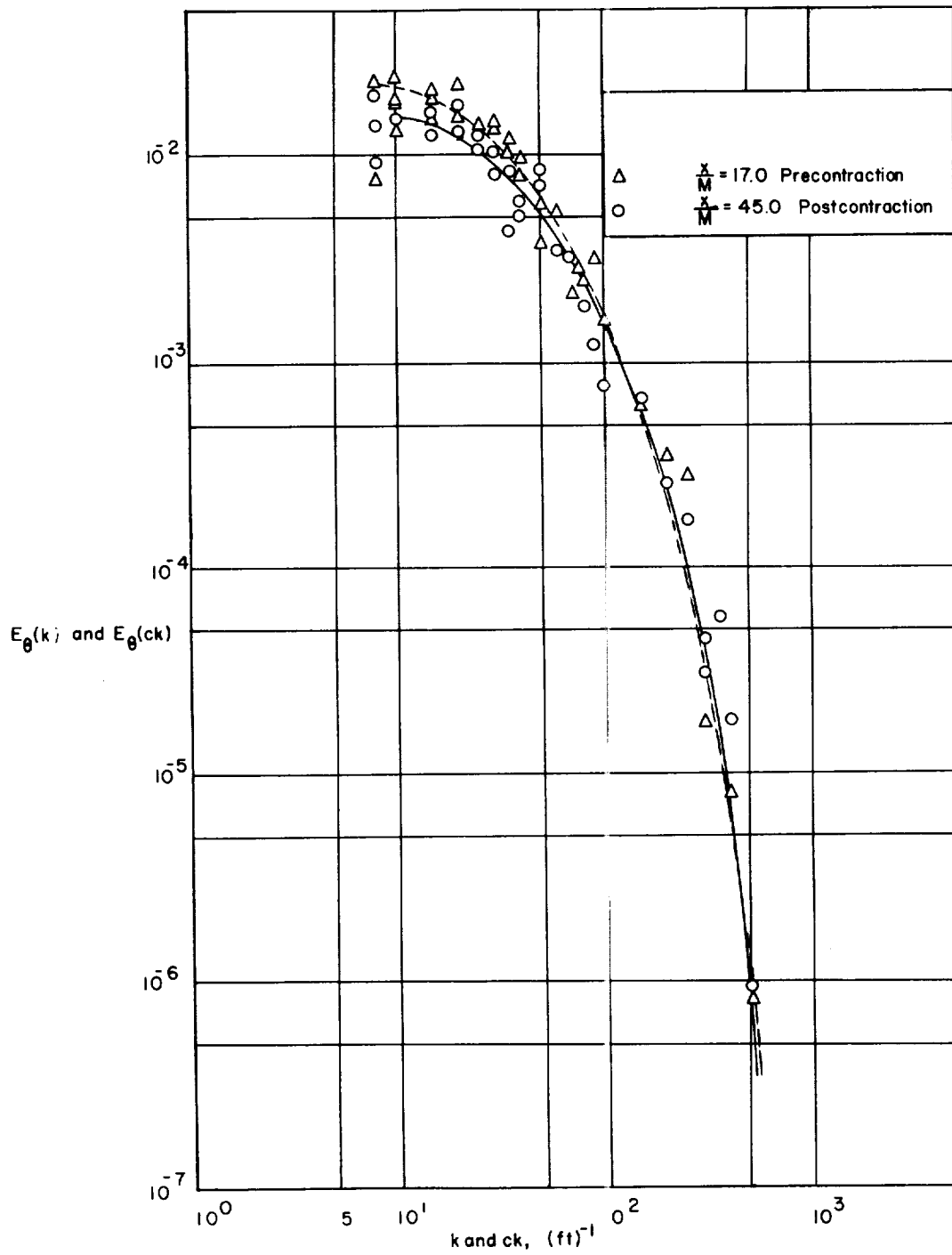
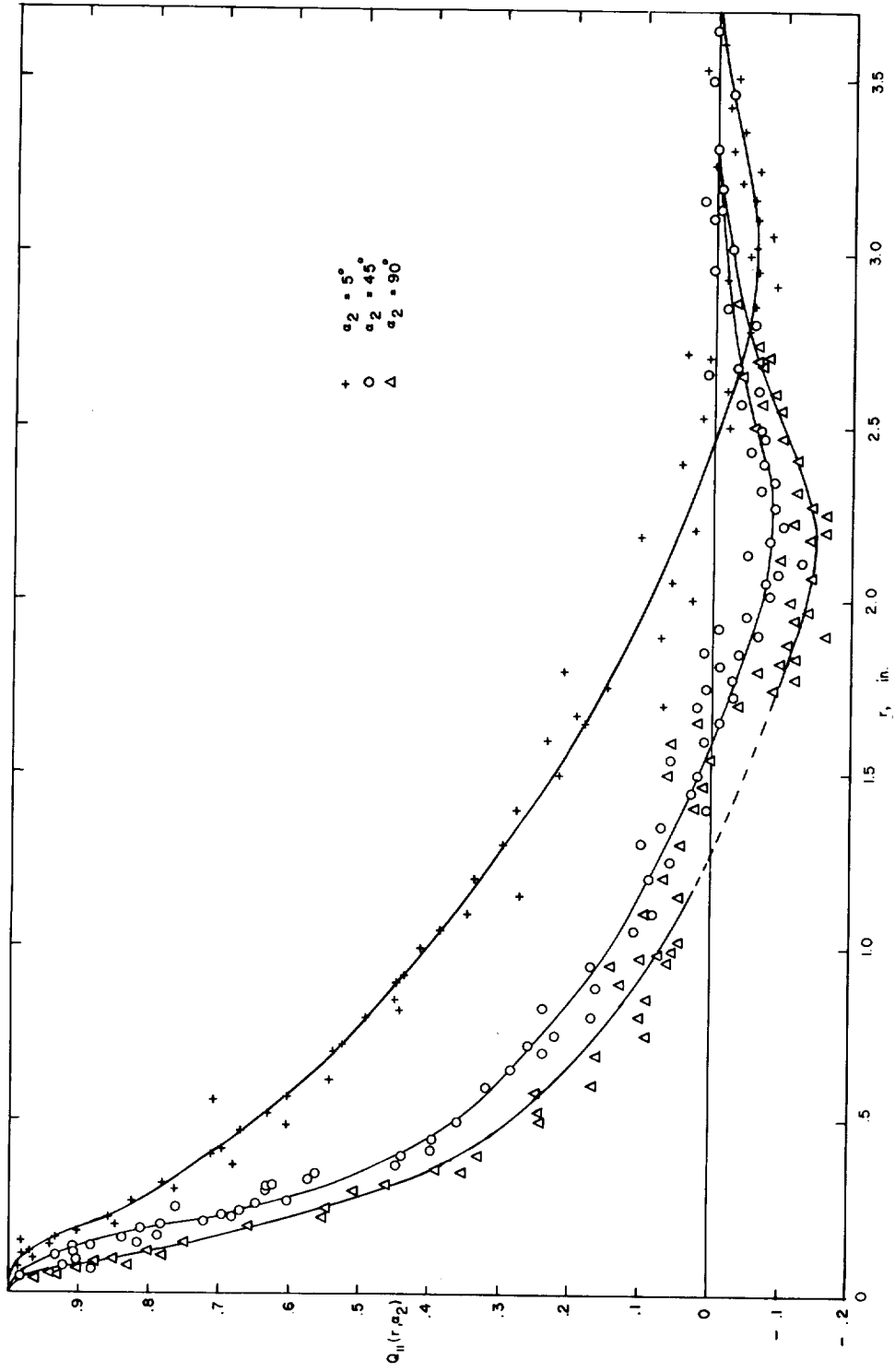
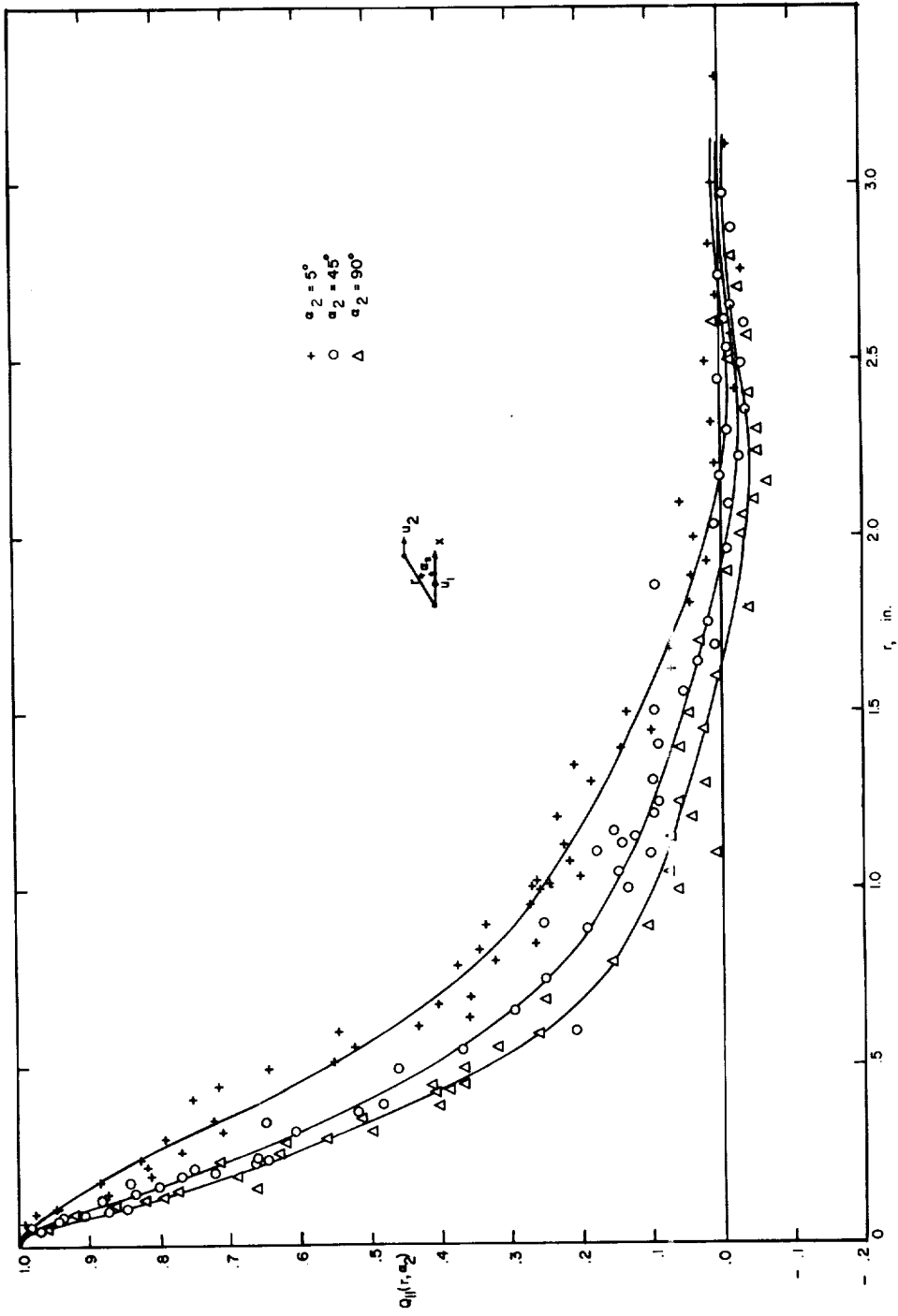
(c) Spectrum of $\overline{\theta^2}$.

Figure 9.- Concluded.



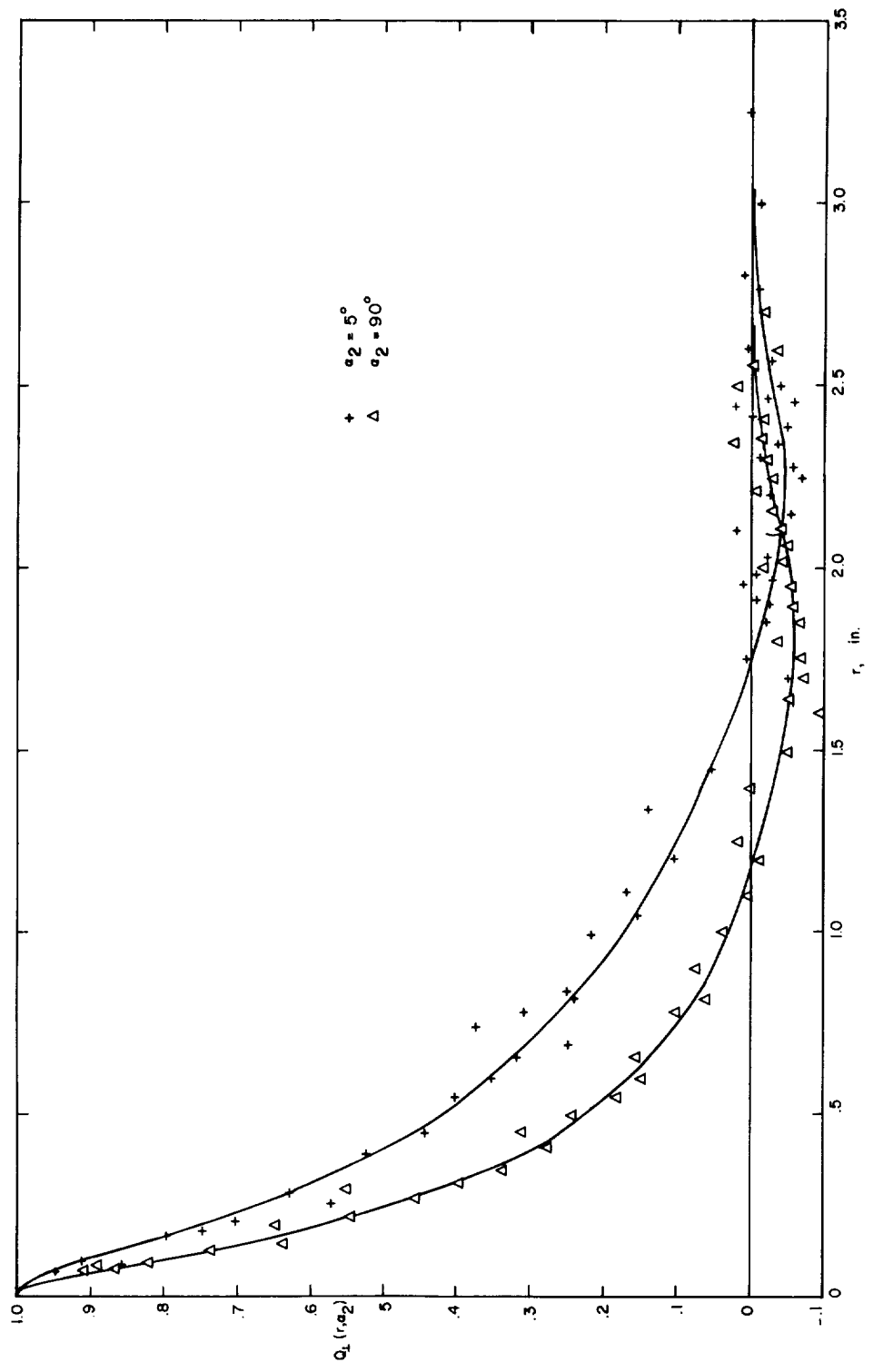
(a) $Q_{11}(r, \alpha_2)$; $\frac{x}{M} = 45$; $\frac{t\bar{U}}{M} = 27.0$.

Figure 10.- Double- and triple-correlation functions downstream of contraction at $x/M = 45$ and 73.



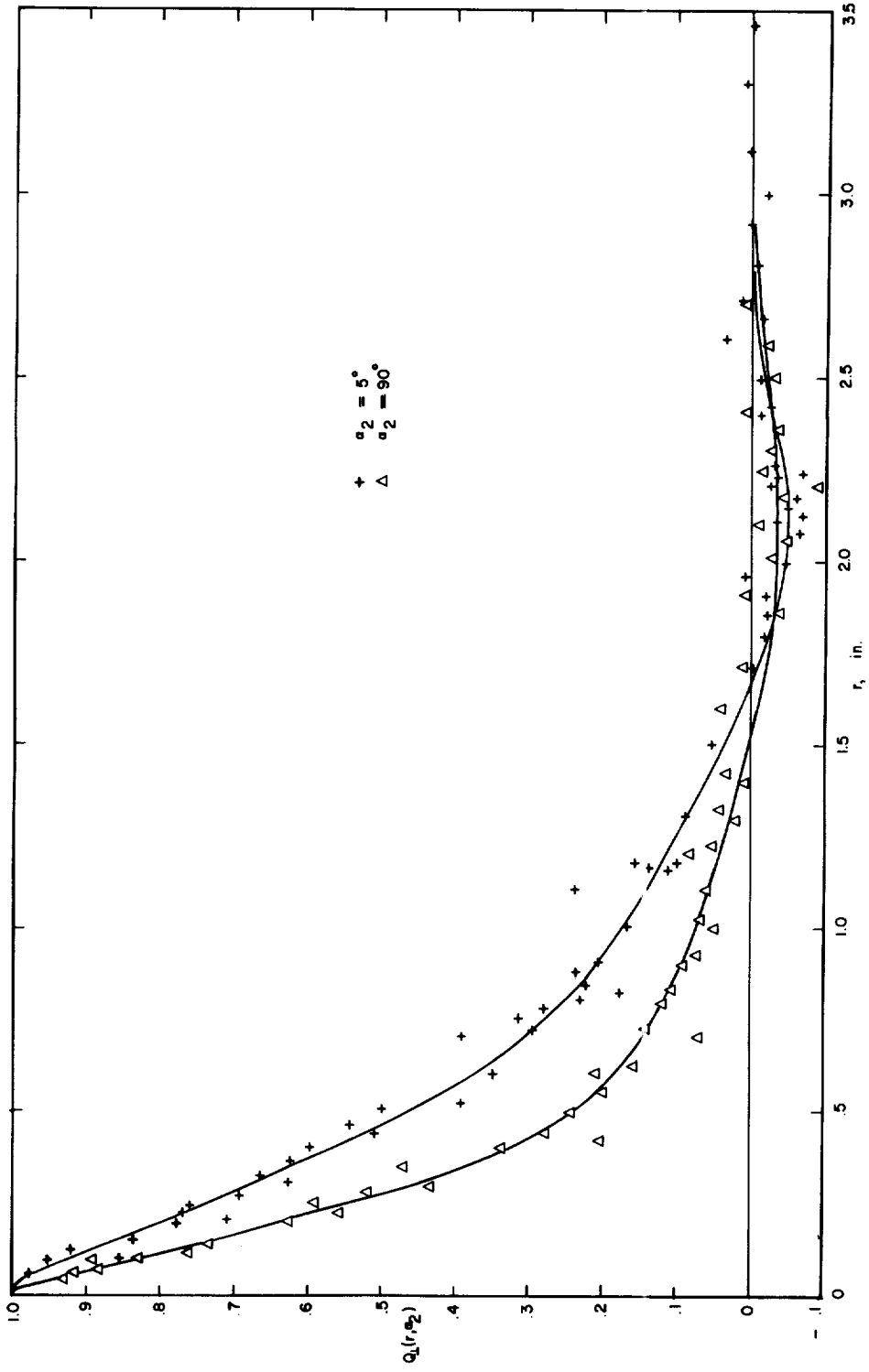
(b) $Q_{||}(r, \alpha_2) = \frac{\overline{u_1 u_2}}{u_1 u_2}; \frac{x}{M} = 73.0; \frac{t \overline{u_1}}{M} = 34.0.$

Figure 10.- Continued.



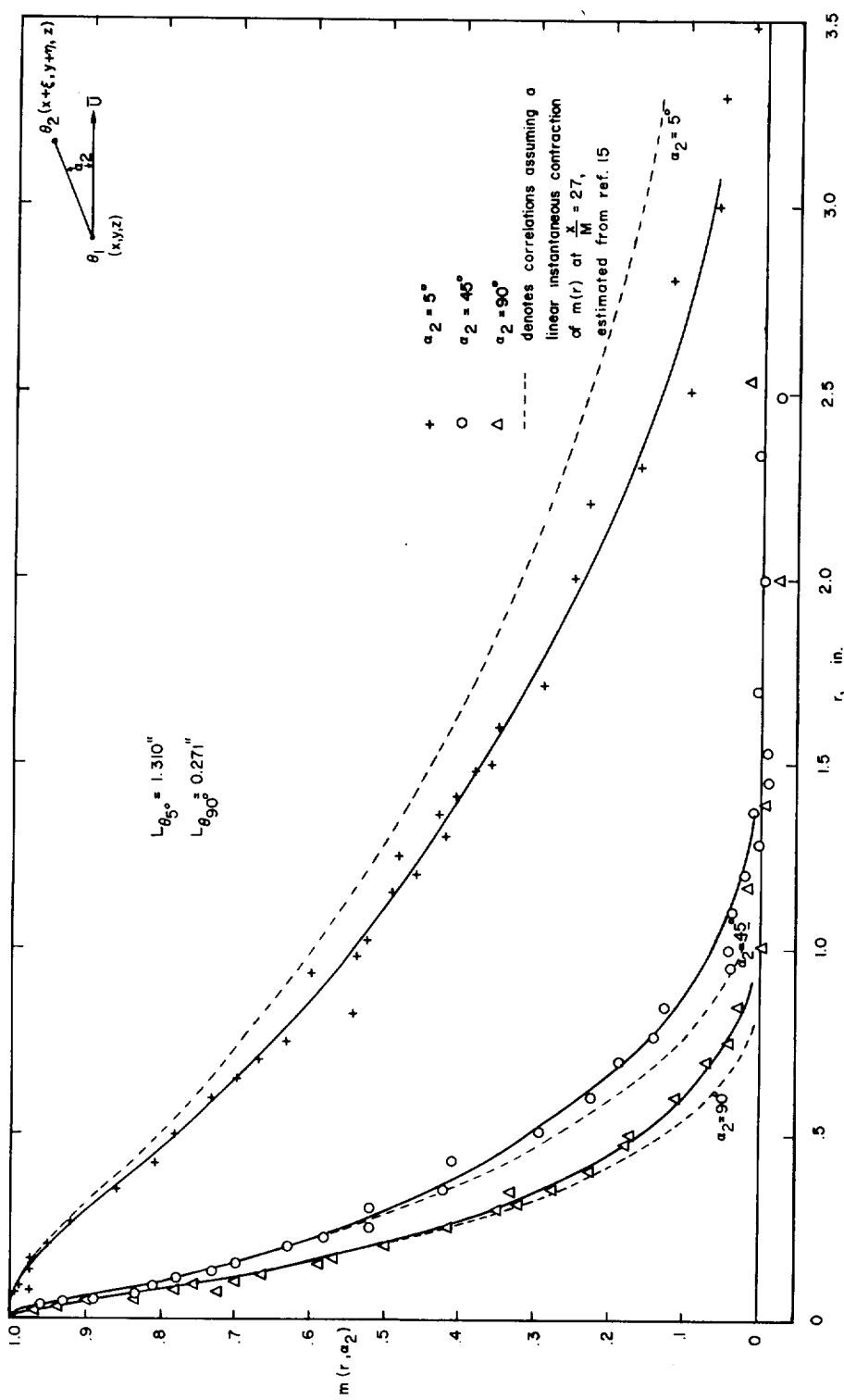
(c) $Q_1(r, \alpha_2); \frac{x}{M} = 45.0; \frac{t\bar{U}_1}{M} = 27.0.$

Figure 10.- Continued.



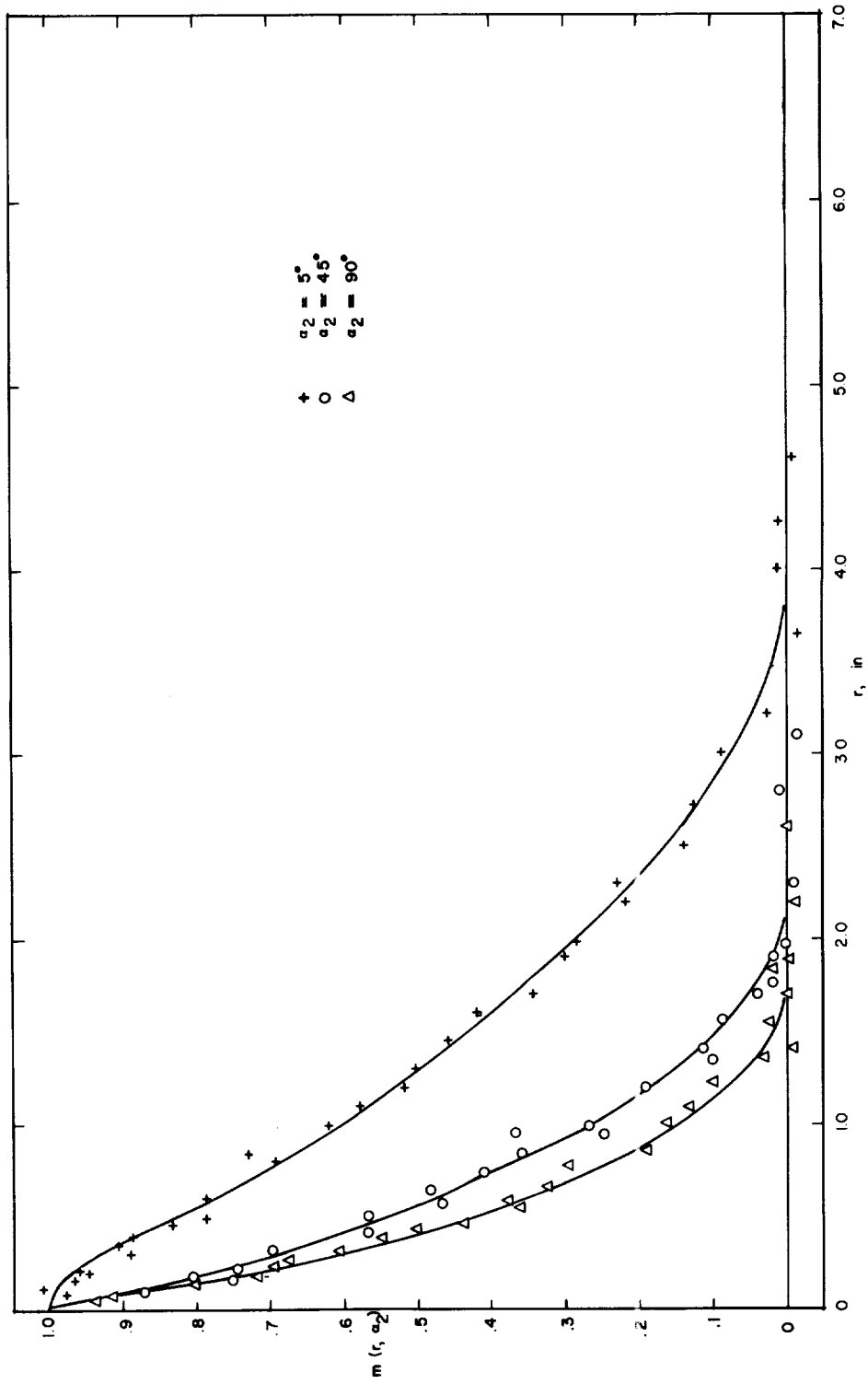
(d) $Q_1(r, \alpha_2)$; $\frac{x}{M} = 73.0$; $\frac{t\bar{U}_1}{M} = 34.0$.

Figure 10.- Continued.



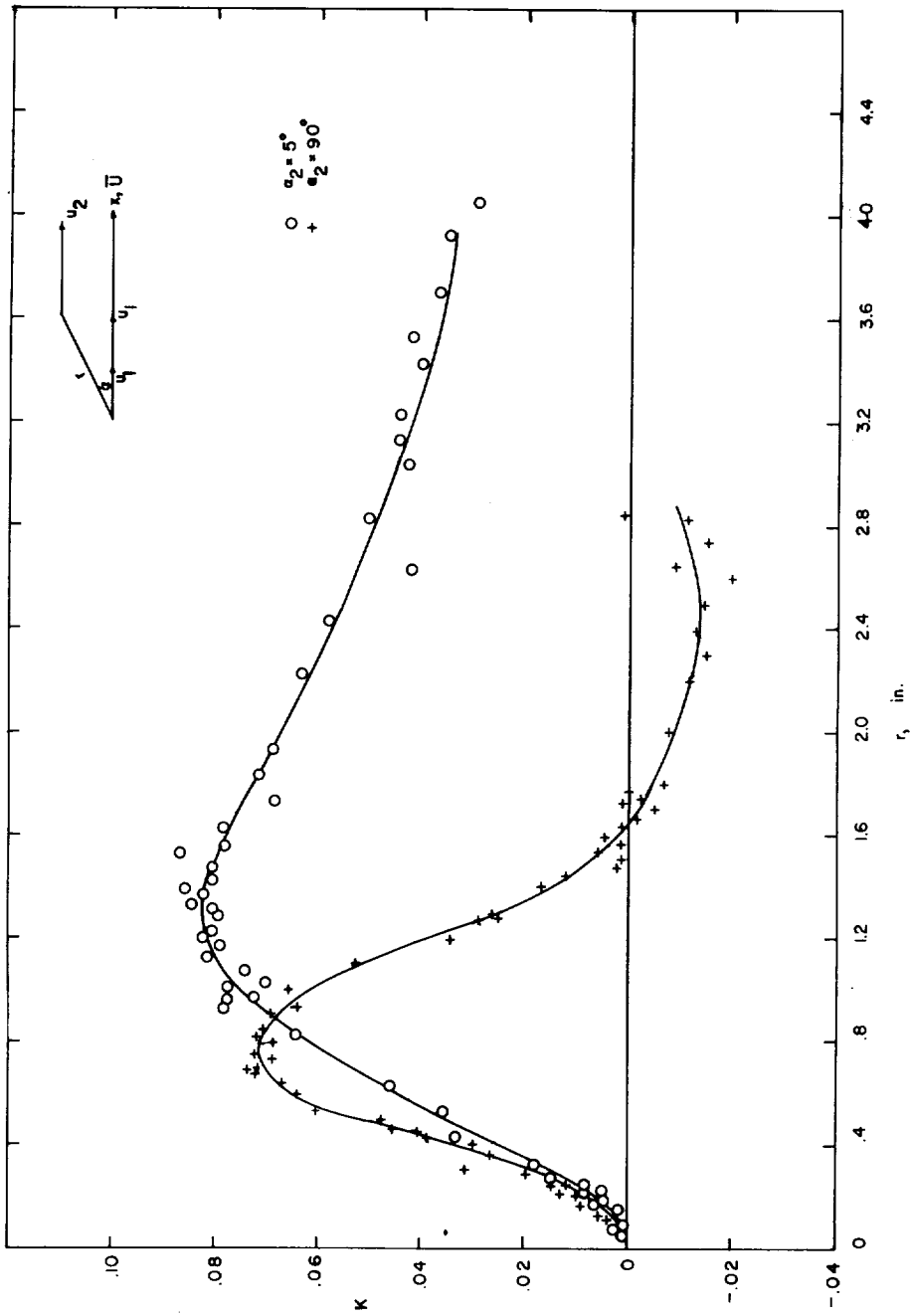
$$(e) \quad m(r, \alpha_2); m(r_1 \alpha_2) = \frac{\overline{\theta_1 \theta_2}}{\theta_1' \theta_2'}; \frac{x}{M} = 45.0; \left(\frac{t\bar{u}_1}{M}\right)_{27.0}^{\text{iso}} = \left(\frac{t\bar{u}_1}{M}\right)_{45.0}^{\text{ax}}$$

Figure 10.- Continued.



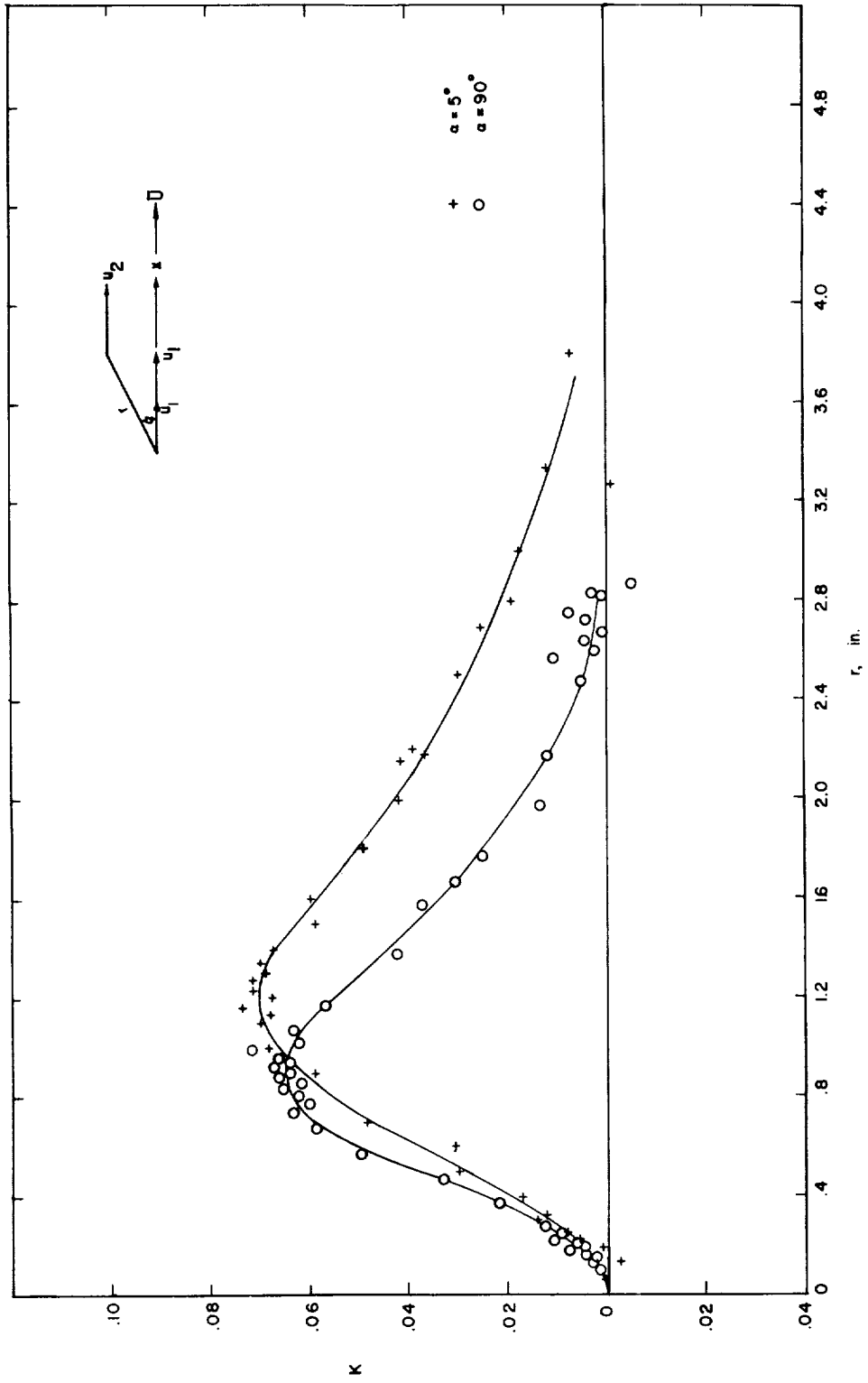
(f) $m(r, \alpha_2)$; $\frac{\lambda}{M} = 73.0$.

Figure 10.- Continued.



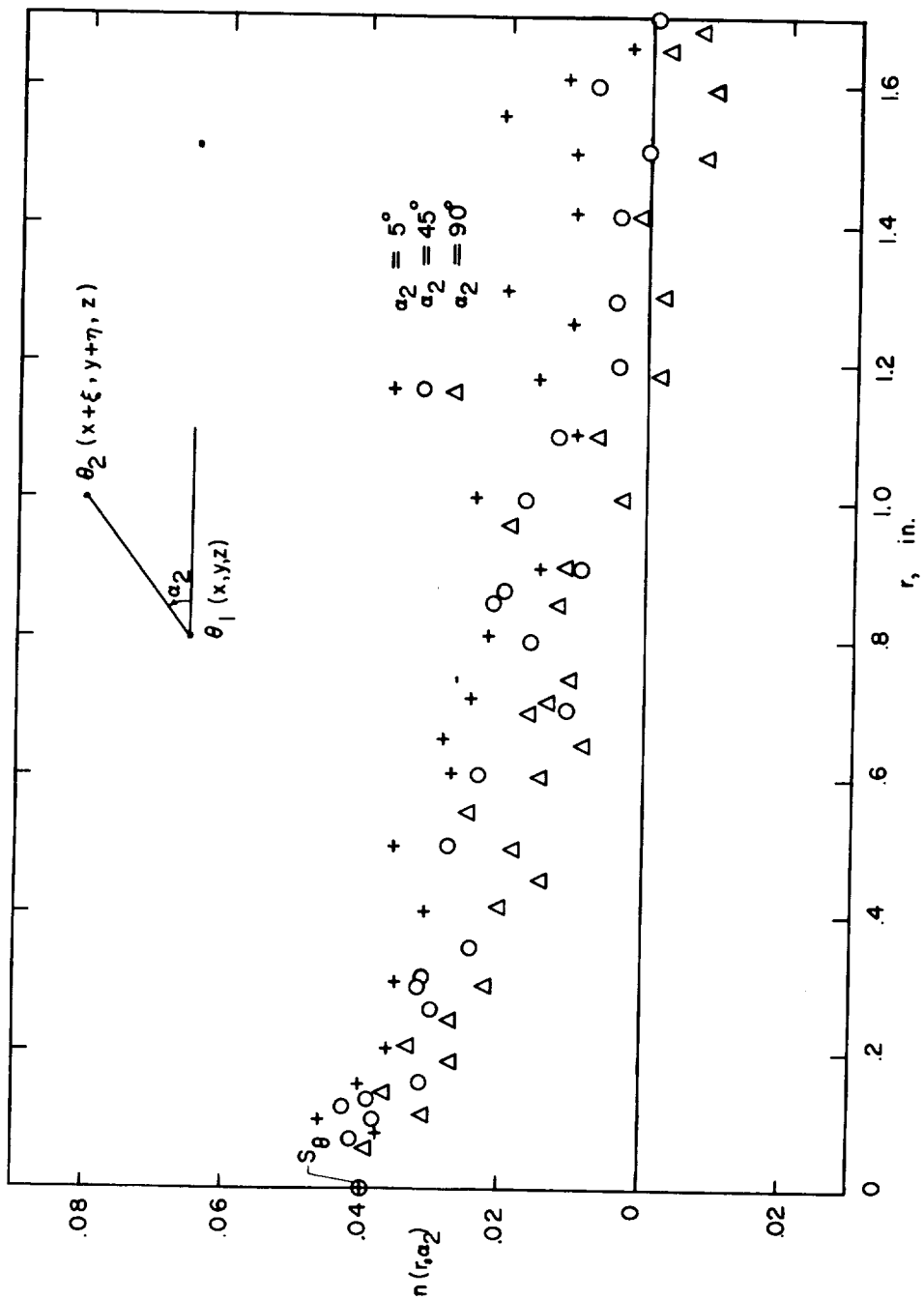
(g) $K = \frac{\overline{u_1^2 u_2}}{u_1^2 u_2'}$; $\frac{x}{M} = 45.0$.

Figure 10.- Continued.



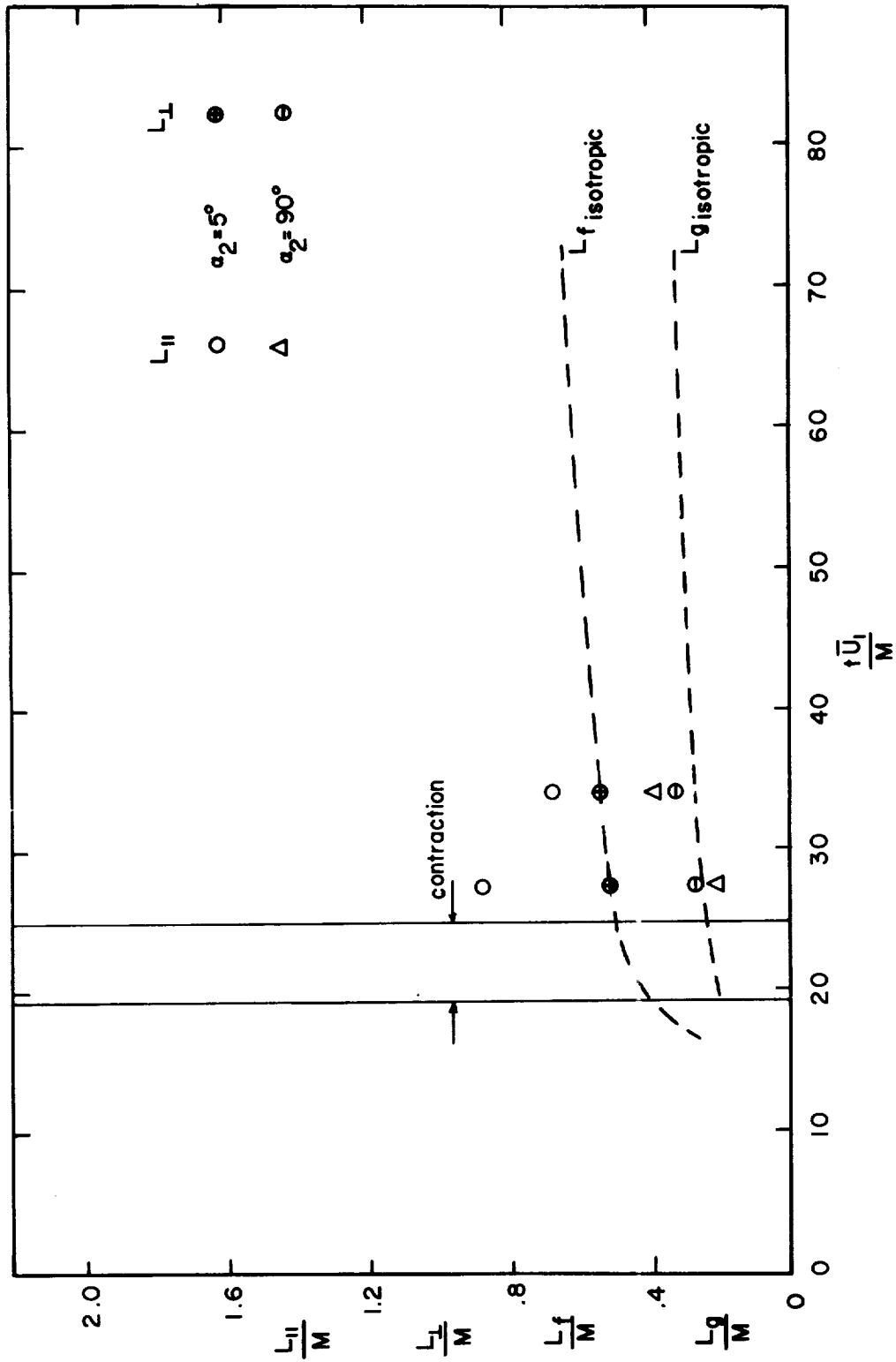
(h) $K = \frac{\overline{u_1^2 u_2}}{u_1^2 u_2'}$; $\frac{x}{M} = 73.0$.

Figure 10.- Continued.



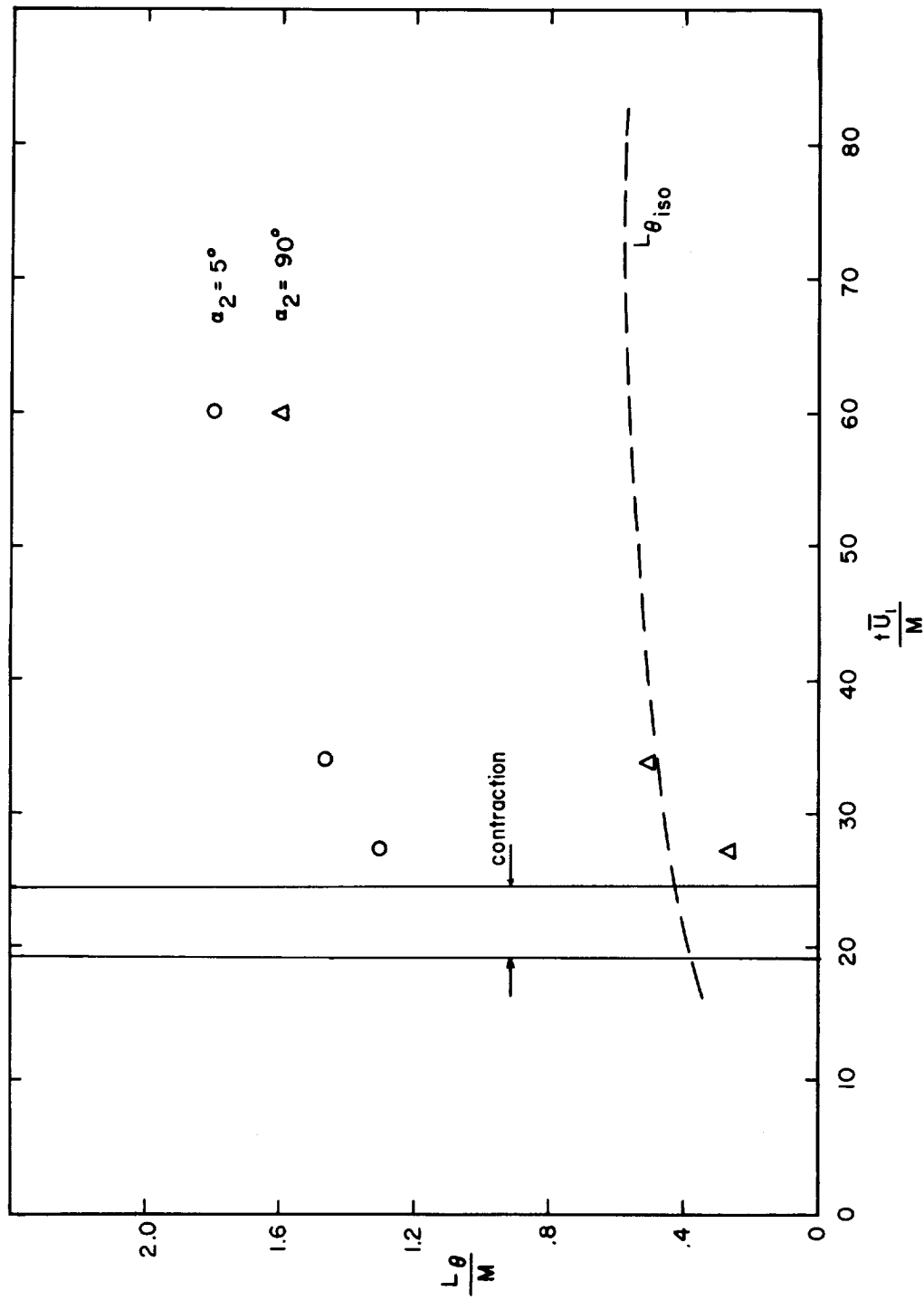
(i) $n(r, \alpha_2) = \frac{\overline{\theta_1^2 \theta_2}}{\theta_1^2 \theta_2'}$; $\frac{x}{M} = 45.0$.

Figure 10.- Concluded.



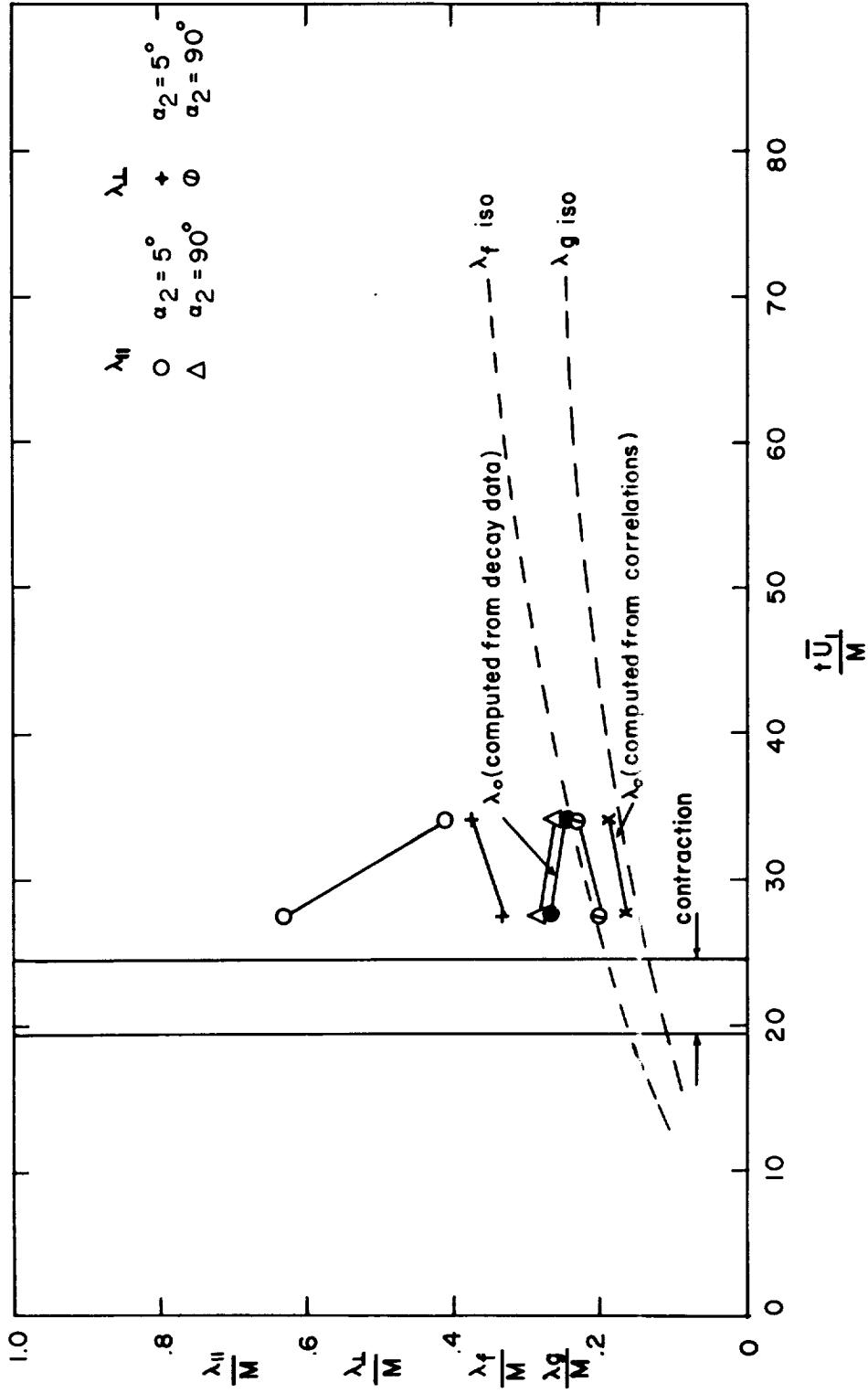
(a) Velocity integral scales.

Figure 11.- Comparison of integral scales of random fields. Curves taken from reference 15.



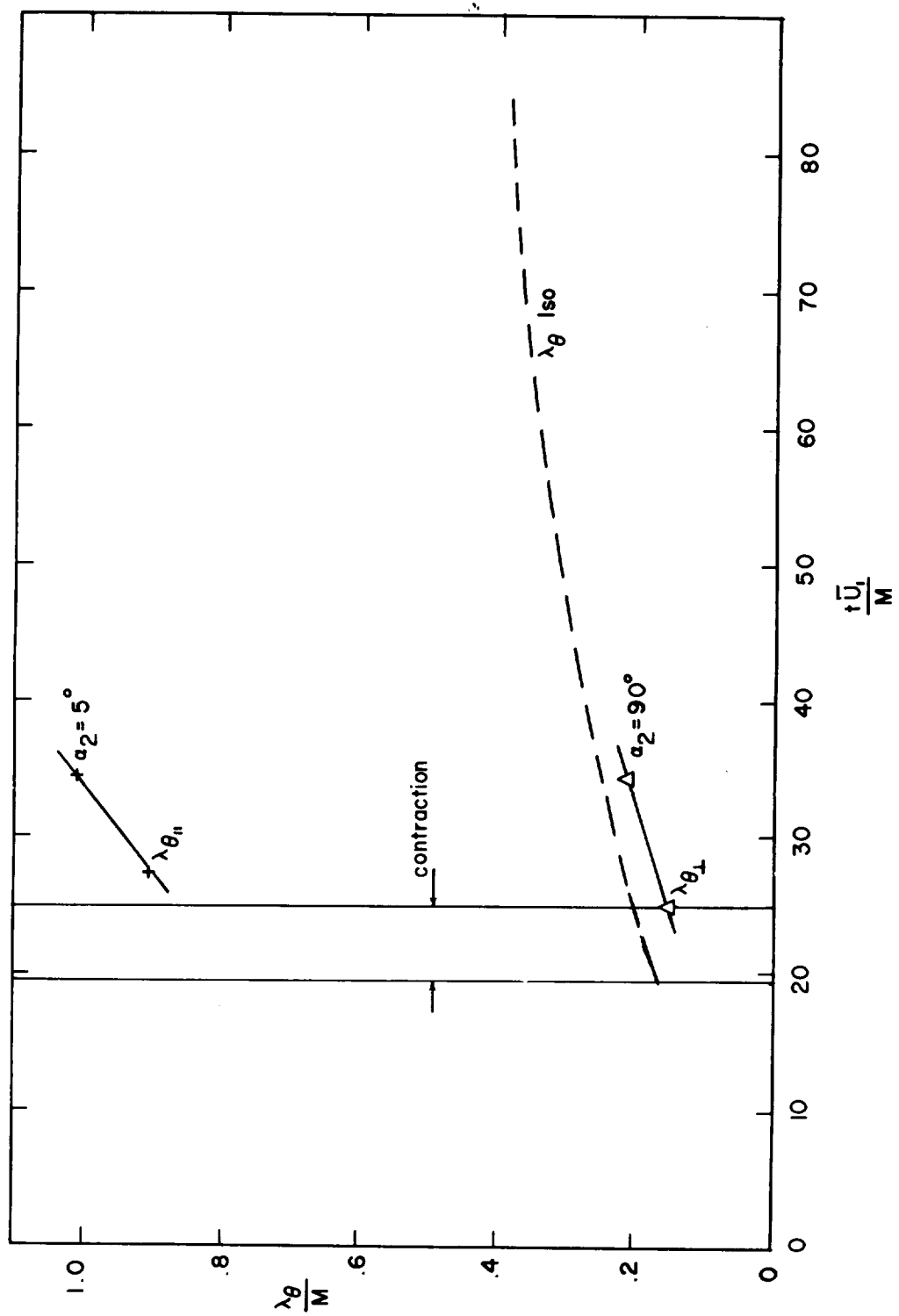
(b) Thermal integral scales.

Figure 11.- Concluded.



(a) Velocity dissipative scales.

Figure 12.- Comparison of dissipative scales of random fields. Curves taken from reference 15.



(b) Thermal dissipative scales.

Figure 12.- Concluded.

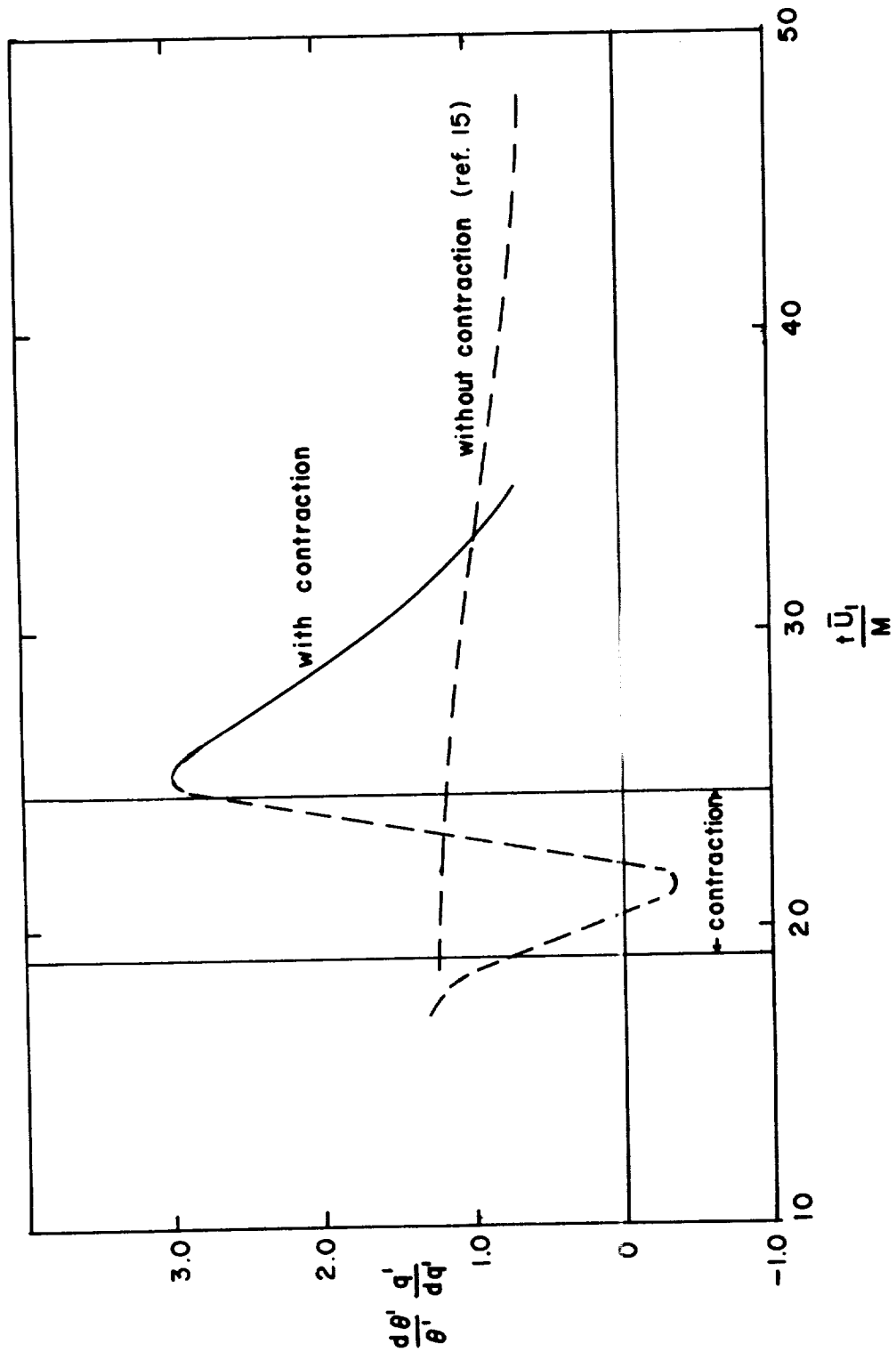


Figure 13.- Relative decay rates of temperature and velocity fluctuations.